



**Fermi National Accelerator Laboratory**

**TM-1616**

# **Mechanical and Thermal Behavior of a Prototype Support Structure for a Large Silicon Vertex Detector (BCD)**

**Hal Mulderink**

*LaGrange High School  
LaGrange, Illinois 60525*

**Neil Michels**

*Apple Valley High School  
Rosemont, Minnesota 55068*

**Hans Jöstlein**

*Fermi National Accelerator Laboratory  
P.O. Box 500, Batavia, Illinois 60510*

**August 23, 1989**



**Mechanical and Thermal Behavior  
of a Prototype Support Structure  
for a Large Silicon Vertex Detector  
(BCD)**

**Hal Mulderink, LaGrange High School, LaGrange, Il. 60525**

**Neil Michels, Apple Valley High School, Rosemount, Mn. 55068**

**Hans Jöstlein, Fermilab**

## **Abstract**

The Bottom Collider Detector (BCD) has been proposed as a device to study large numbers of events containing B mesons. To identify secondary vertices in hadronic events it will employ the most ambitious silicon strip tracking detector proposed to-date.

This report will discuss results from measurements on a first mechanical/thermal model of the vertex detector support structure. The model that was built and used for the studies described here is made of brass. Brass was used because it is readily available and easily assembled by soft soldering, and, for appropriate thicknesses, it will behave similarly to the beryllium that will be used in the actual detector. The trough was built to full scale with the reinforcement webbing and the cooling channels in place. There were no detector modules in place. We plan, however, to install modules in the trough in the future.

The purpose of the model was to address two concerns that have arisen about the proposed structure of the detector. The first is whether or not the trough will be stable enough. The trough must be very light in weight yet have a high degree of rigidity. Because of the 3m length of the detector there is question as to the stiffness of the proposed trough. The main concern is that there will be sagging or movement of the trough in the middle region. The second problem is the heat load. There will be a great deal of heat generated by the electronics attached to the detector modules. So the question arises as to whether or not the silicon detectors can be kept cool enough so that when the actual experiment is run the readings will be valid. The heat may also induce motion by differential expansion of support components.

Although further testing is necessary, at this point in time one of the two questions has been answered. From the data and results that will follow it appears that the proposed construction is stable and that the sagging or movement in the detector will be small enough. The thermal issue is, as of this time, not resolved. The initial results are encouraging but further testing is needed.

Since the experiment is still ongoing at this time it will not be the purpose of this report to answer either of the proposed questions but to present the data and experiments that have been performed.

1. IntroductionThe Bottom Collider Detector (Fig. 1) has been proposed to study the full range of physics associated with the production of large numbers of B-antiB pairs. It is estimated that the Tevatron p-anti-p collider could produce  $10^{11}$  B-anti B pairs per year <sup>1</sup>. This many events would allow for complete and thorough study of the B system in detail which has not been done previously. Many measurements will be taken and knowledge gained on the way to the major goal of this program which will be to study CP violation in the B system.

## 2. Description of the Vertex Detector

The silicon vertex detector is essential in extracting the B signal in a high-multiplicity environment. The current plan is to use 0.2 mm-thick silicon, with double sided readout for the detectors. The silicon detector modules will be hexagonal as shown in figures 2, 3 and 4. Also shown in the figures is the position of the amplifier and readout chips, which are the major source of heat in the assembly. There is also a 1 inch diameter beam pipe which will be made of beryllium.

---

<sup>1</sup>" Letter of Intent for the BCD - A Bottom Collider Detector for the Fermilab Tevatron" , October 7, 1988.

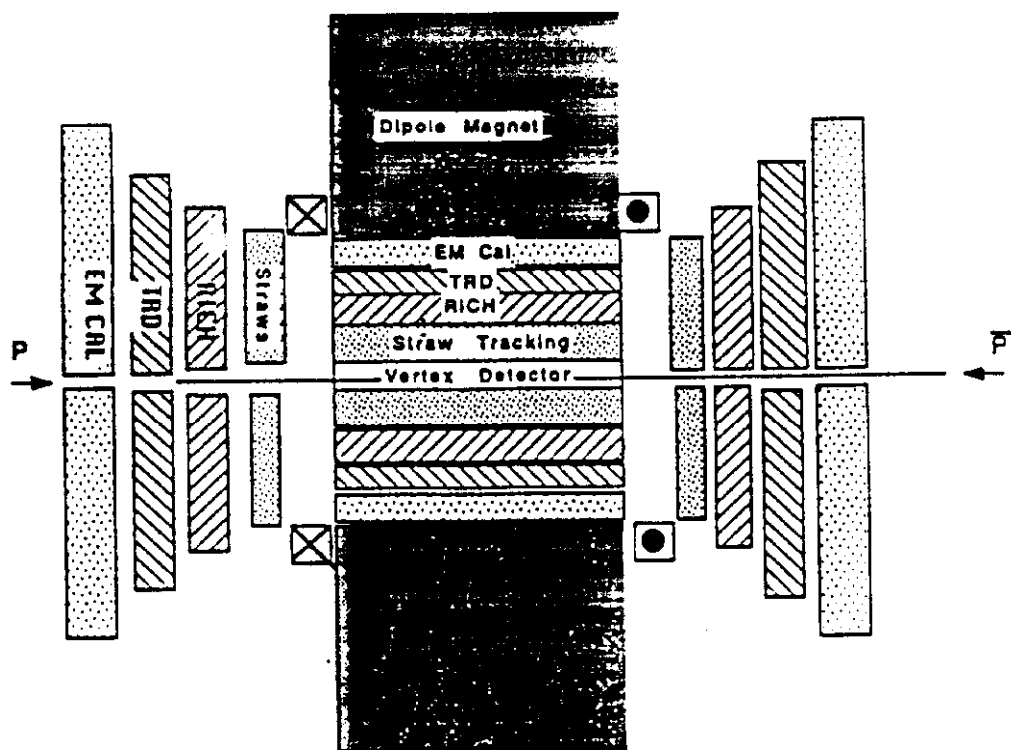


**Fig. 1 Overview of the BCD Detector**

BCD SILICON VERTEX DETECTOR  
CENTRAL STATIONS  
FULL SIZE

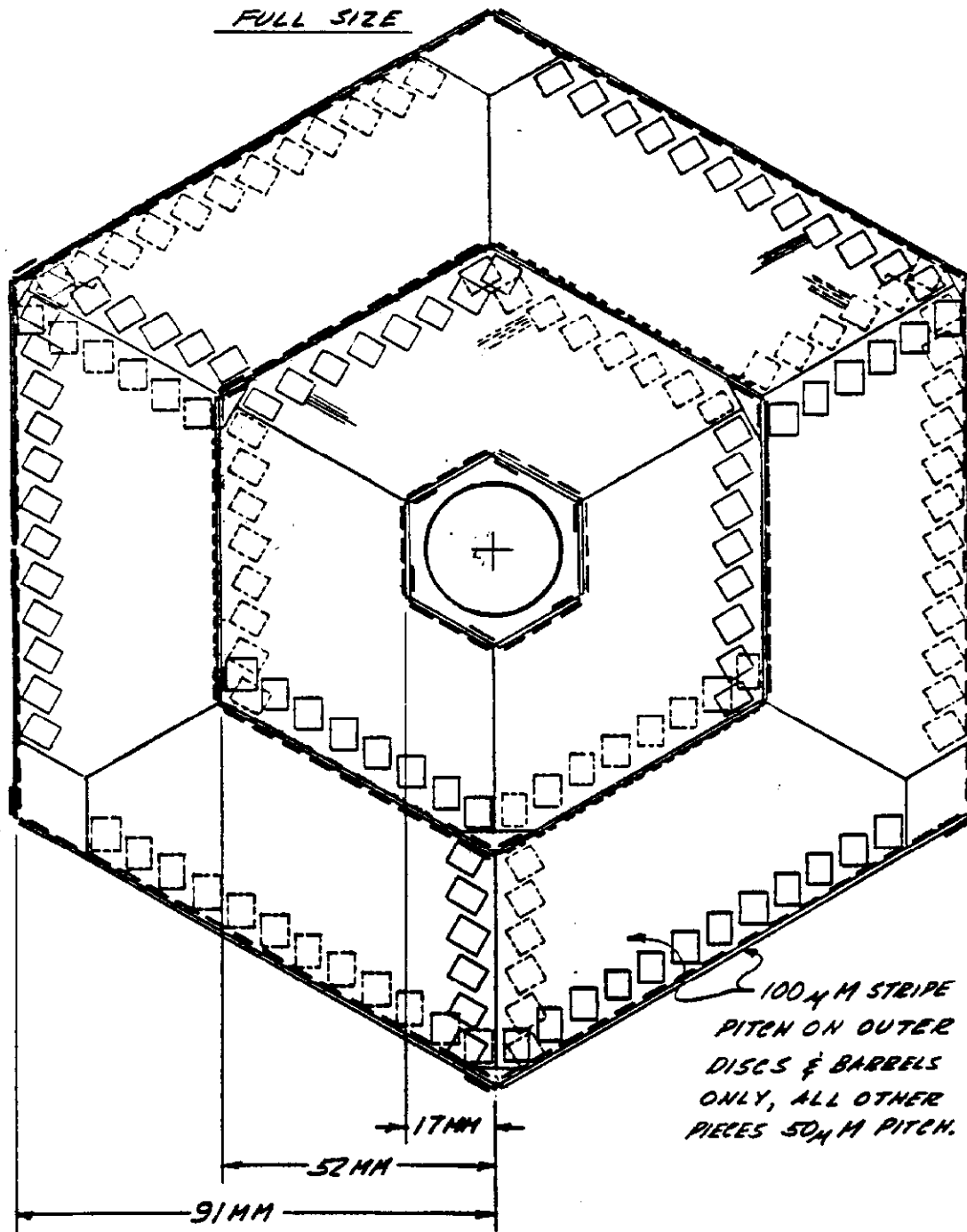


Fig. 2 BCD Silicon Vertex Detector, Central Stations

4 3-4-89

# BCD SILICON VERTEX DETECTOR FORWARD STATIONS

A 25% REDUCTION IN NO OF CHANNELS IN THE  
FORWARD SECTION CAN BE REALIZED IF THE  
REDUNDANT STRIPES ARE NOT INSTRUMENTED.

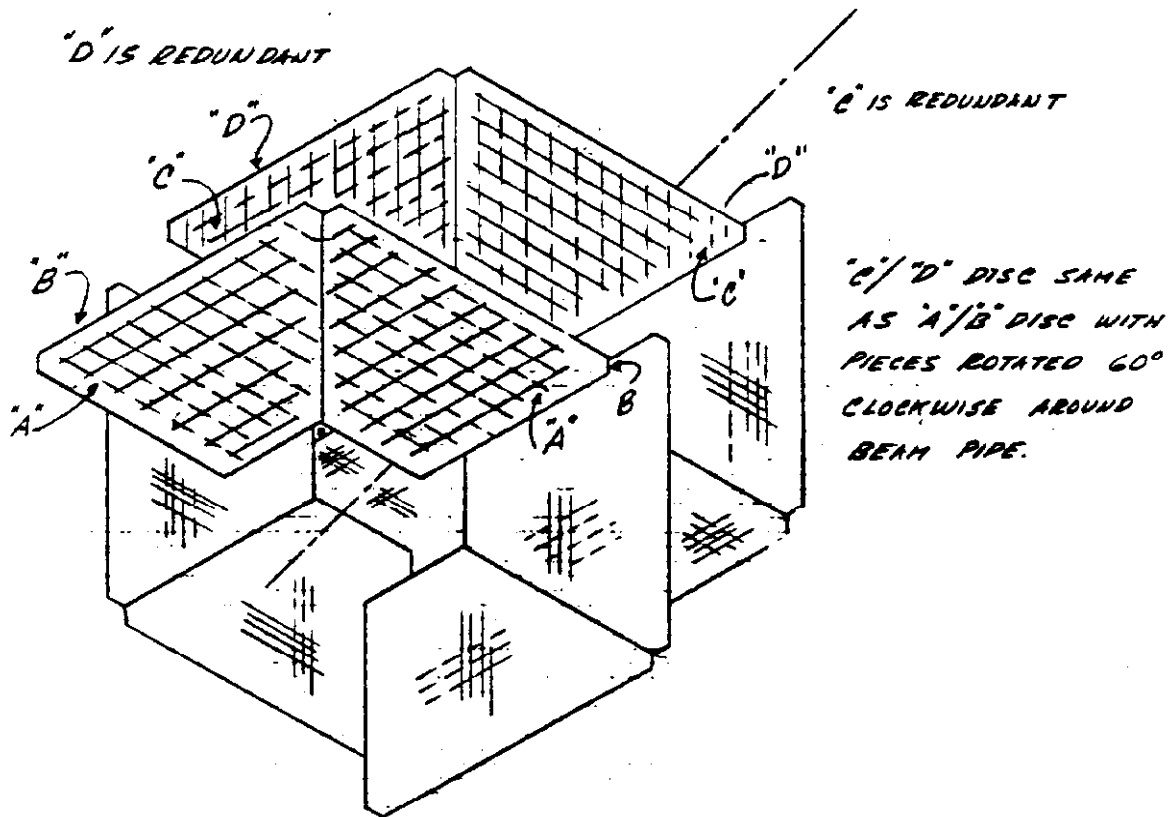


Fig. 3 BCD Silicon Vertex Detector, Forward Stations

4-3-4-89

BCD SILICON VERTEX DETECTOR  
FORWARD STATIONS  
FULL SIZE

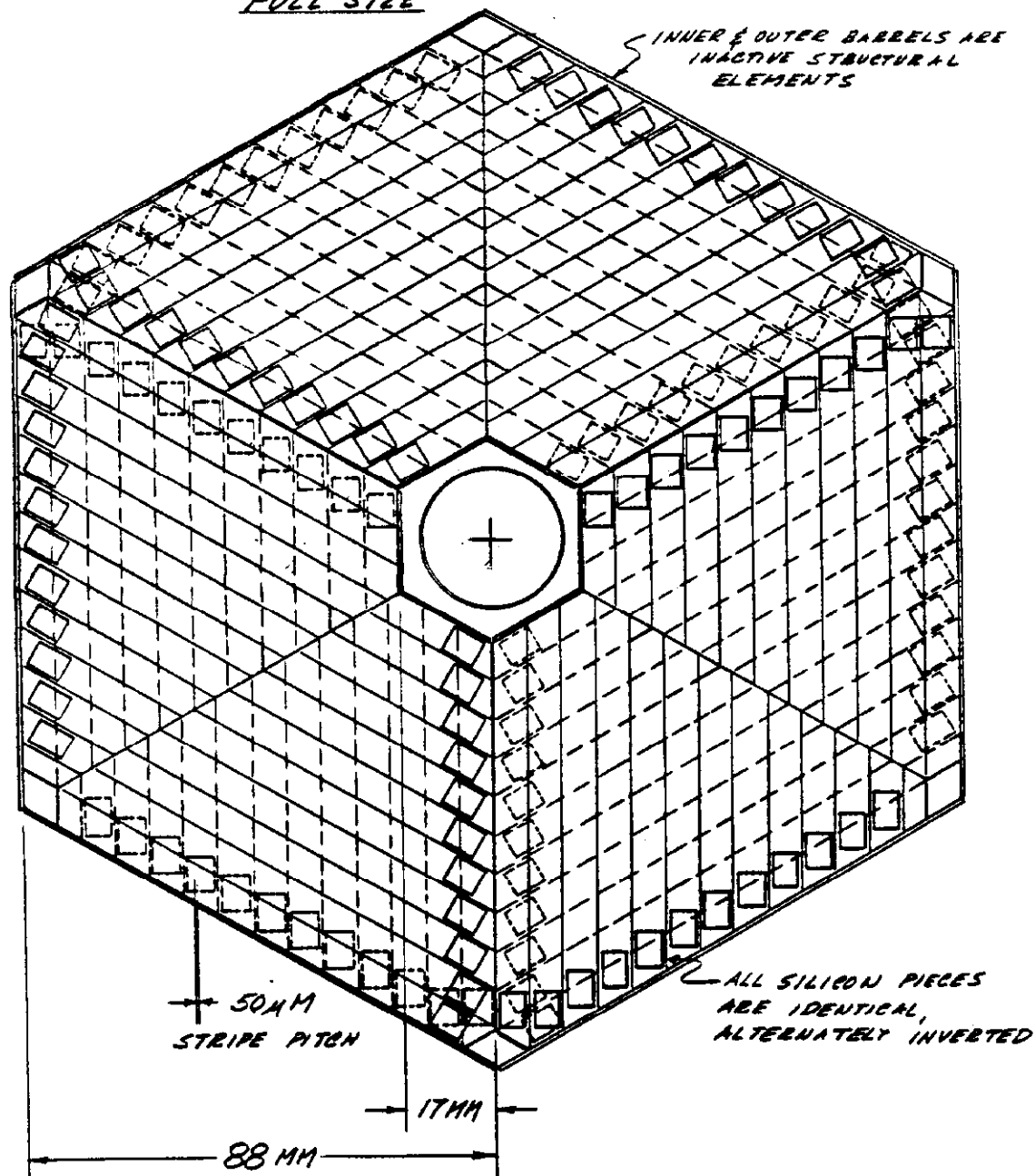


Fig. 4 BCD Silicon Vertex Detector, Forward Stations

The silicon detectors consists of all-silicon self supporting modules which will be mounted in a trough or "gutter" 304.8 cm long which will be made from beryllium approximately 0.254 mm (10 mils) thick. The structure will be reinforced by beryllium webbing brazed across the gutters between the silicone detector modules. Attached to the outside of the trough will be four channels which will provide additional stiffening and will serve as a coolant channel. Figure 5 shows how the detector modules will be mounted in the trough<sup>2</sup>.

### **Required Stability**

The basic accuracy scale is given by the stripes defining a channel on a silicon detector chip. These stripes vary in width from as low as 25 microns for the innermost barrel to 100 microns on the outer barrel.

If the whole assembly moves as a unit, however, vertex reconstruction is not very seriously impaired, and the transverse beam dimensions (100 m microns typically) set the scale of accuracy.

Furthermore, if a motion occurs slowly or infrequently, one can envision to update the trigger and reconstruction constants to keep track of the motions.

Hence the level of concern is around 100 microns (= 4 mils) of motion.

---

<sup>2</sup> All Figures provided by Carl Lindenmeyer

4-5-89

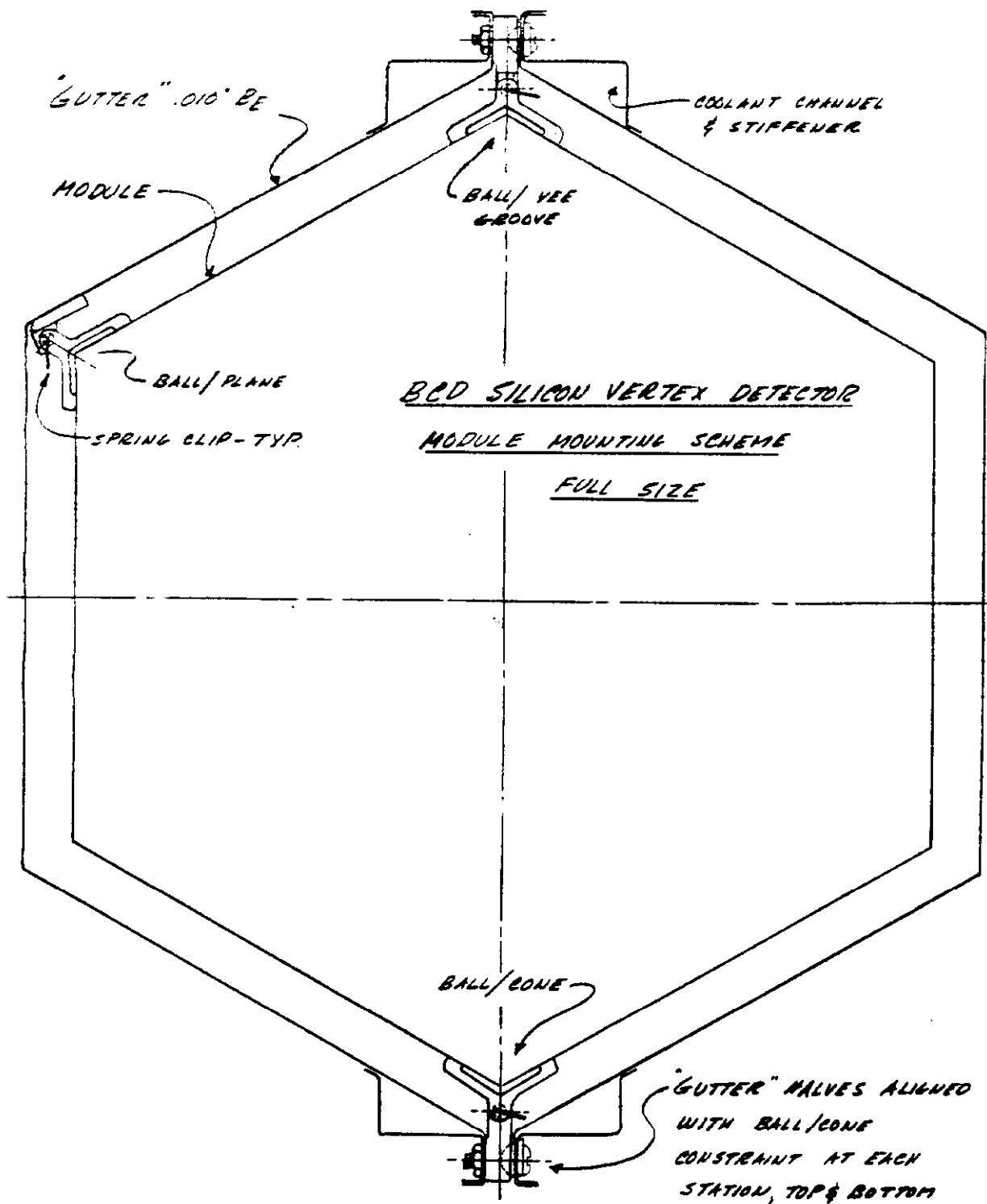


Fig. 5 BCD Silicon Vertex Detector, Module Mounting Scheme

### 3. The Mechanical/Thermal Model and the Test Equipment

#### 3.1 Choice of Material (Brass versus Beryllium)

The final support structure is expected to be a brazed beryllium assembly of 10 mil wall thickness. This minimizes multiple scattering while maximizing stiffness and thermal conductivity.

Beryllium is very expensive and hard to work with. We chose to make the present model out of 10 mil brass. Brass is easily soldered into the desired configuration.

In analyzing the following data it is important to compare how the actual chamber made from beryllium will perform in comparison to this model.

The **elastic modulus** of brass is  $16 \times 10^6$  lbs/in<sup>2</sup> while the modulus of beryllium<sup>3</sup> is much higher,  $42 \times 10^6$  lbs/in<sup>2</sup>. The rigidity, or resistance to sagging, of beams of rectangular cross section depends directly on the elastic modulus and the cube of the material thickness (both the proposed chamber and the brass model are 10 mils thick). As an example:

$$\text{RIGIDITY FACTOR} = \text{MODULUS} \times (\text{THICKNESS})^3$$

$$\text{Beryllium} = 42 \times 10^6 (0.010)^3 = 42$$

$$\text{Brass} = 16 \times 10^6 (0.010)^3 = 16$$

$$\text{Stiffness comparison: Brass/Beryllium} = 0.38$$

This comparison applies to solid beams. The main support structure (the gutters) is a box beam of hexagonal cross section. Its stiffness is linear in both wall thickness and modulus of elasticity.

---

<sup>3</sup> "Materials Engineering", December 1980

As can be seen from these calculations the actual detector will be more than twice as rigid as the model.

The **thermal expansion coefficient** of brass, beryllium and other relevant materials is listed in Fig. 6. Brass expands at  $20.5 \times 10^{-6} / ^\circ\text{C}$ , while beryllium expands less,  $11.3 \times 10^{-6} / ^\circ\text{C}$ . The brass model will, if anything, show larger motion than a similar beryllium structure will.

Some of the heat will be conducted through the brass walls to the cooler water moving through the water channels. In comparing the **thermal conductivities** we find:

Heat Conductivity of Beryllium = 87 Btu-ft/hr-ft<sup>2</sup>-°F

Heat Conductivity of Brass = 70 Btu-ft/hr-ft<sup>2</sup>-°F

one can see that the conductivity of the brass is 79% of the beryllium that will be used. Thus brass will not have the same ability to cool the chamber air via the water channels as the proposed beryllium support.

### 3.2 Mechanical Structure of the Model

The two halves of the support structure (called troughs or gutters because of their resemblance to rain gutters on houses) were formed out of brass 10 mils thick. The troughs were 120 inches long and the three flat faces of each are about 4.5 " wide. Edges were provided along each side of the gutter to enable the two troughs to be joined together. Webbing was then soldered into each of the troughs to stiffen them, to aid in heat transfer, and to support the module mounts. The webs were made of brass 12 mils thick. Holes were cut into the webs to allow for air flow through the chamber (the actual proposed webs would have larger openings). What the webs will look like in the chamber after the troughs are joined together is shown in Fig. 7:

MATERIAL	COEFFICIENT OF THERMAL EXPANSION $\times 10^{-6}/^{\circ}\text{C}$	REMARKS
SILICON	2.6	+20°C TPRC
PYREX	2.8	+20°C TPRC
GRANITE (DIBASE)	6.3	RAWH, STANLEY ETC.
ALUMINUM NITRIDE	2.1	$\left. \begin{array}{l} @ -55^{\circ}\text{C} \\ @ +125^{\circ}\text{C} \end{array} \right\}$ COORS
" "	3.8	
" "	4.1	
SILICON NITRIDE	2.0-1.4	20-400°C STD. OIL
" "	2.5-2.6	25-200°C GTE
SILICON CARBIDE	3.9-5.4	0-400°C KYOCERA
MILD STEEL	15.1	0-400°C KYOCERA
304 STNLS. STL.	14.7	MAT'L HANDBOOK
440 STNLS. STL.	9.5	+20°C TPRC
BERYLLIUM	11.3	+20°C TPRC
COPPER-C10200	17.6	+20°C TPRC
BRASS-C36000	20.5	MAT'L HANDBOOK
ALUMINUM-6061	23.4	MAT'L HANDBOOK
KAPTON	20	DU PONT
G-10 X-Y	16.2-12.6	NVF
	9.9	$\left. \begin{array}{l} 15 \text{ MOST COMMON} \\ \text{VALUE USED} \end{array} \right\}$
	9	
	14-18	
CERAMICA	7	OAK
EPOXY KEVLAR LAMINATE	X-Y 6	MAT'L HANDBOOK
"	Z 62	ELECT. PKG. & PROD. MFG.
MICROY 1100	9.36	HERCULES 0-26°C MICAPLY
CORLAM	3-7	ARLON <sup>®</sup> NI-4093
		" "
		MICROY/MICALEX
		DUPONT (KEVLAR / EPOXY)

Fig. 6 Coefficient of Thermal Expansion for Various Materials

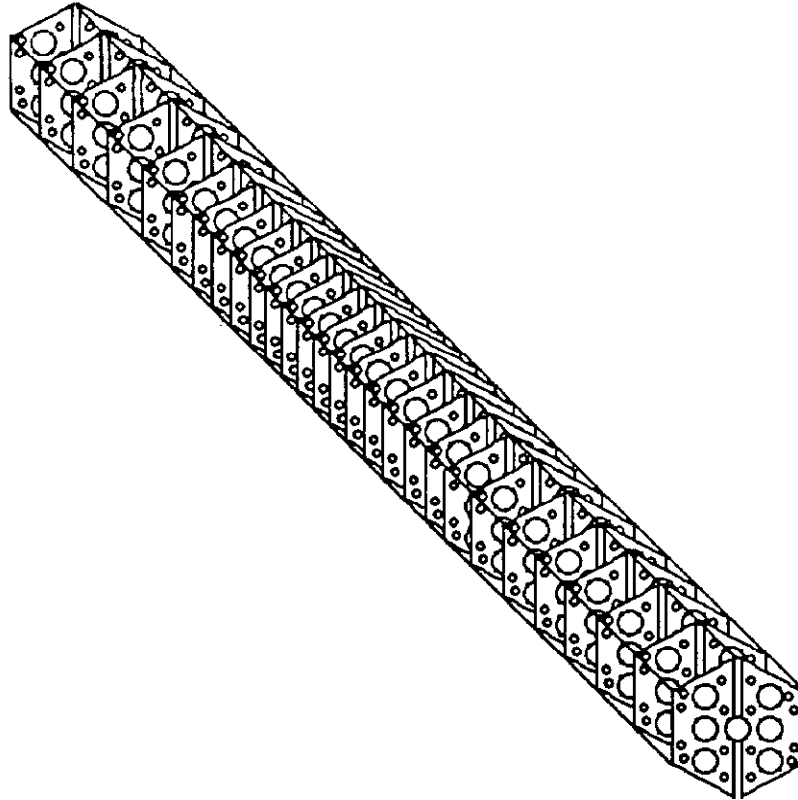


**Fig. 7      Arrangement of Reinforcing Webs in the Gutters**

After the webs were installed, four water channels were soldered to the outer skin of the troughs. The channels were made out of 10 mil brass.

### 3.3 Mechanical Assembly and Support

To assemble the two halves of the trough holes were drilled every six inches in each of the edges of the troughs. The troughs were then placed side-by-side so that the line joining them is in a vertical plane. Aluminum shims were placed between the edges of the two troughs. The shims were 6" long x .75" wide x .25" thick. The troughs were bolted together by #8 machine screws. To get a more uniform pressure from the screws along the trough pieces of G-10 and rubber were used between the head of the screw and the brass and also between the nut and the brass. The G-10 and rubber pieces were 1.5" x .5" x .125". The troughs were then bolted to two aluminum stands, one at each end of the chamber, as shown in Fig. 8:

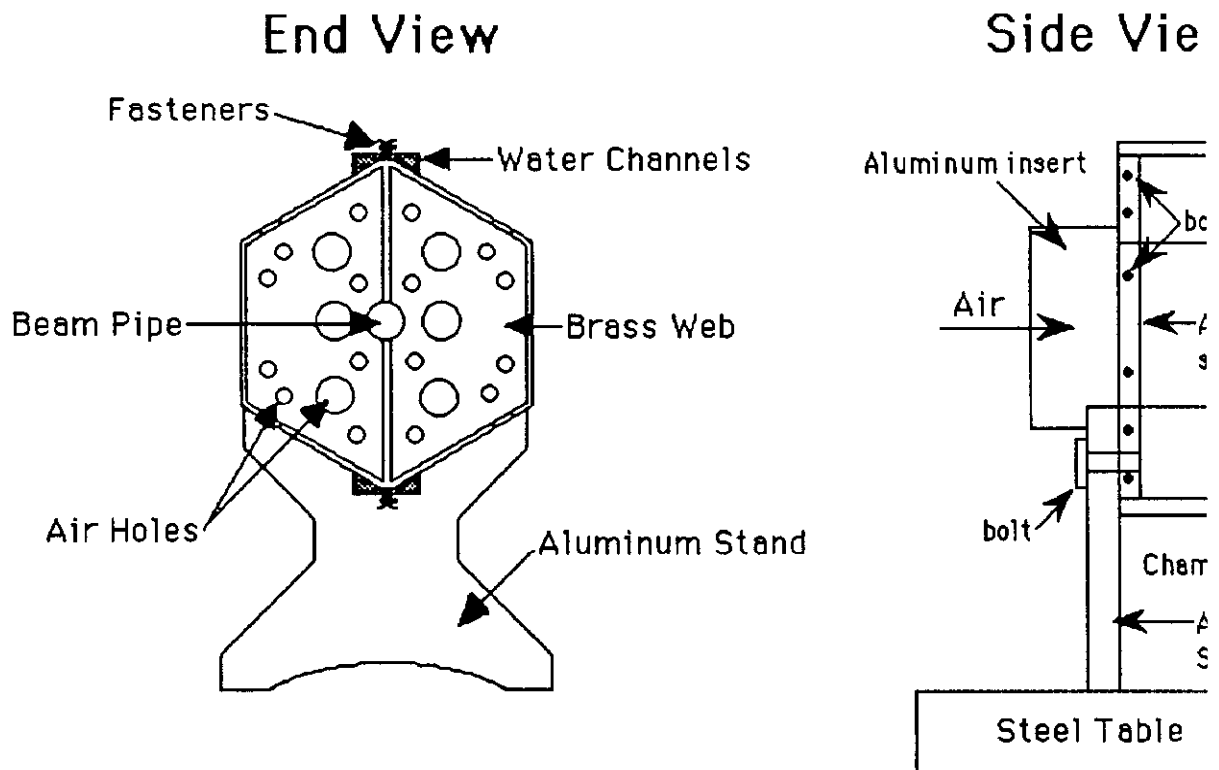


Fig. 8 Mounting Stand Design

The stands were initially both made from aluminum 0.625" thick. Both stands were epoxied or clamped to the steel table. This may have induced vertical bowing due to thermal expansion during some of the runs, as discussed later. Consequently the downstream stand was later replaced by one made from 1/16" thick aluminum.

A six inch opening was provided in each of the stands to permit the passage of air through the chamber. The stands are 17" high and when the chambers are mounted on them the bottom of the chamber is 6.75" above the surface. The supporting base was a "magnet table" which consists of a steel box beam with one inch thick top and bottom plates, separated by eight inches.

### **3.4 Heating Strips**

Silicon rubber heating strips were then placed in one of the troughs. The heating strip specifications and type are:

Watlow - St. Louis #010300C1

120 Volts (AC)      150 Watts

8831C              1 LT

Eight strips were used so at maximum voltage 1200 watts of power will be generated. To simulate the heat output distribution of the signal amplifiers, the strips were concentrated along the center of the trough, thus concentrating the heat output in the middle of the chamber(see Fig. 9). The parallel resistance of all the heat strips connected in the chamber was 12.2 ohms, as measured on a Beckman Industrial, HD 110, digital multimeter.

### **3.5 Air Cooling Fans**

The cooling of the chamber during the experiments was done by moving air through the chamber, by placing a fan at one end, and/or moving cooled water through the water channels.

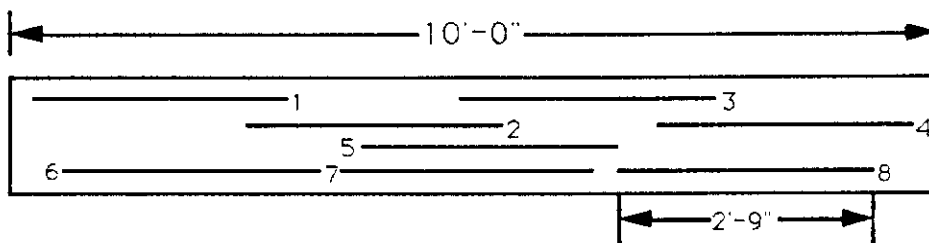


**Fig. 9 Heating Strip Placement**

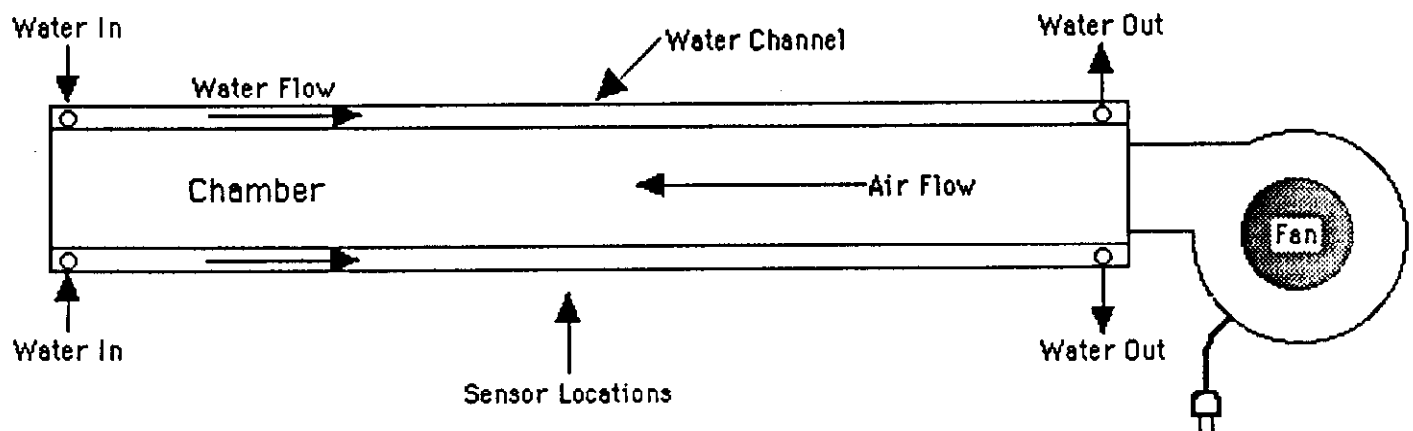


**Fig. 10 Air and Water Cooling Configuration**

Three different fans, of increasing flow capacity, have been used in the testing:

<b>Fan Name</b>	<b>Diameter</b>	<b>Manufacturer</b>	<b>Mass Flow</b>
Boxer Fan	4.5"	imc Magnetics	24 g/s
Centrifugal Blower	8 "	Æ	58 g/s
Turbine	14"	Nederman, 0.65 hp	120 g/s

### **3.6 Water Cooling**

The water was moved through the channels by a centrifugal pump made by Dayton Electronics, model #1p956, and cooled by a refrigeration unit made by the Blue M Electric company, model number PCC-13A-3. The water flow rate was 50 g/s.

The air and water cooling configuration is shown in Fig. 10 .

### **3.7 Thermometry**

Ten air temperature sensors were placed in the chamber. The sensors were first inserted in a 1" Ø aluminum pipe which had about one-third of its circumference removed to admit air to the sensors. The wiring was then enclosed in G-10 for safety and to make insertion of the probes easier. The first and last sensors are 6 inches from the ends of the chamber and all sensors are 12 inches from each other. The temperature sensors were integrated circuit, temperature sensors #LM34CAZ. The basic principle behind the temperature sensor is that when wired to a low voltage source it produces a DC output voltage proportional to the temperature in Fahrenheit (at 10 mV/F).

Similar sensors were also installed to measure the lab air temperature, the steel table temperature and the cooling water inlet and outlet temperatures.

### 3.8 Position Sensing

Seven Electro Corporation<sup>4</sup> Electro Mini-Prox Proximity Sensors were then mounted on Magnetic Bases and placed around the center of the chamber. Proximity sensors create a high frequency magnetic field which is damped by any metal target within the sensing range. The amount of damping is converted to a DC output voltage which is a linear function of the target distance. Proximity sensors exhibit no contact force and very low drift (well below 1 mil/week) for the model used.

As shown in Fig. 11, there are two sensors underneath to measure vertical displacement, two on the sides to detect horizontal displacement, the one on the lower left water channel along with the one on the upper right water channel are to determine rotational motion, and the two bottom water channel sensors provide a check for horizontal displacement.

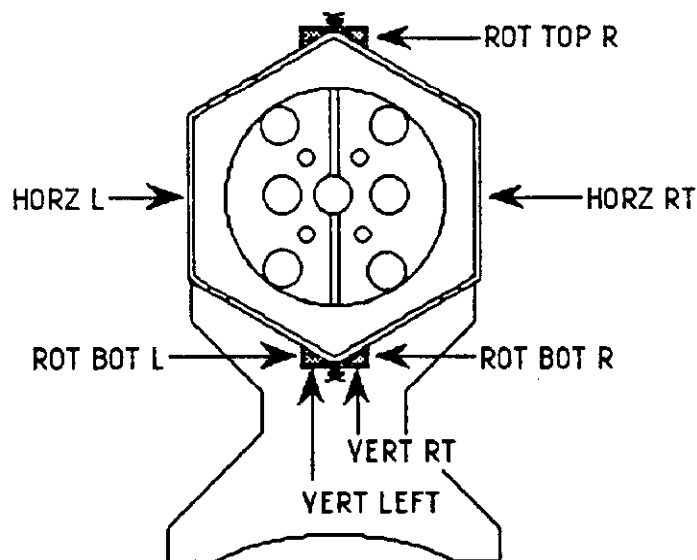


**Fig. 11 Placement of the Proximity Position Sensors**

---

<sup>4</sup>Electro Corporation, P.O. Box 3049, Sarasota, FL 33578

The proximity sensors are each connected to an Electro-Mike Control Module PBA210. The PBA210 is an oscillator/converter module that is designed to convert the signal from the sensor to an output voltage that is directly proportional the distance from the sensor to a metallic target.

### 3.9 Data Acquisition

All the data in this report, collected from both the temperature and proximity sensors, is recorded directly into a Macintosh SE via an IOtech Macintosh/IEEE 488B Bus (GPIB bus) Controller, as shown in Fig. 12. The bus controller operates a Keithley 705 Scanner which has two Keithley 7064 Low-Voltage Scanner cards plugged into it. The cards are wired to the temperature sensors and the PBA210 so they can receive their output signal. The signals are read with a Keithley DMM196 Digital Multi-Meter, also on the GPIB bus, and connected to the scanner.

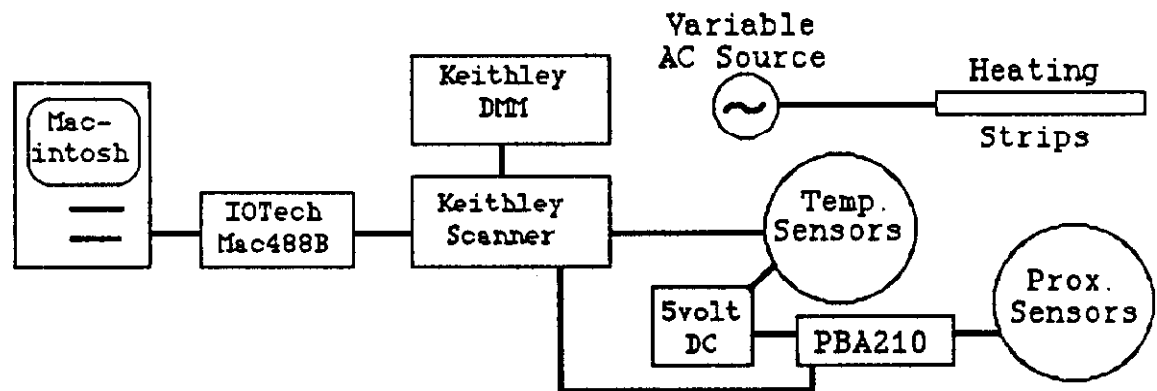


Fig. 12 Schematic of the Data Acquisition System

## 4. Sensor Calibration

### 4.1 Proximity Sensor Calibration

Prior to calibration of the proximity sensors the output voltage range in the PBA210 modules was set by varying the resistance in the circuit as per manufacturer's specifications. It was desired to have as large a range as possible within the recommendation that the maximum output voltage be set at 10 V. The minimum output was set by placing a piece of brass directly in contact with the sensor and adjusting the  $R_g$  potentiometer to achieve the lowest possible voltage output. As can be seen from Fig. 13 labeled Proximity Sensor Calibration, the minimum reading was generally around 3.5 V although it ranged from 2.95 to 4.8 V. The maximum output voltage was set with the sensors open to the room and adjusting the  $R_s$  potentiometer until each sensor had an output voltage of approximately 10.5 volts.

The proximity sensors were then calibrated. Five pieces of G10 of varying thickness were attached to brass with five minute epoxy. To determine the distance from the outer surface of the G-10 to the brass under it, the thickness of the combination was measured then the thickness of the brass subtracted. The G-10 was then placed in contact with each sensor and the voltage recorded. Since the G-10 is transparent to the sensor, this method allowed for a direct means of translating the voltage output measured by the DMM to distance. All readings were taken twice and the average values fitted to a straight line. The data are shown in Fig. 13. The gains (in volts/mil) were then entered into the scanning program which monitored the sensors for all of the data taken. It was set up so that all of the distances printed out were in mils. The readings at the starting time of the first run were used as offsets. The program changes the data (in volts) by subtracting the offset then dividing the difference by the gain. For example with proximity sensor #21 (vertical right) a reading of 5.0 Volts would translate to an actual distance of 27.416 mils:

$$\text{Dist(mils)} = (5.0\text{V} - 1.9234\text{V}) / .11222 \text{ V/mil} = 27.416 \text{ mil}$$

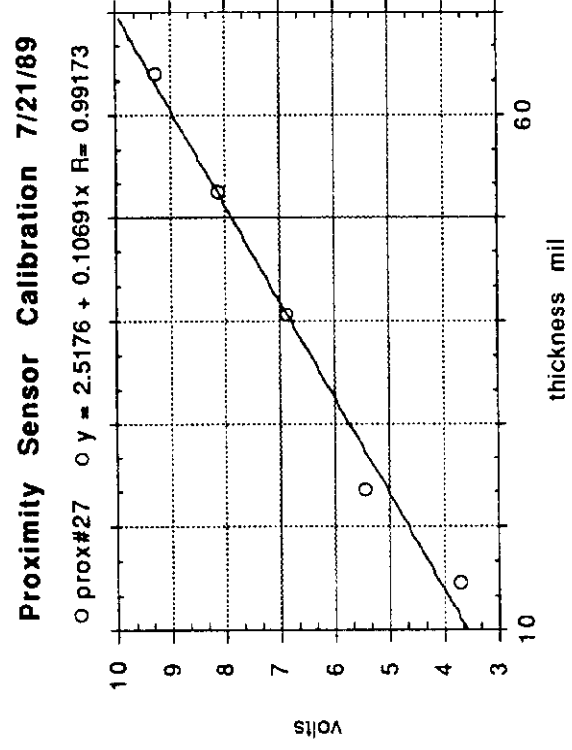
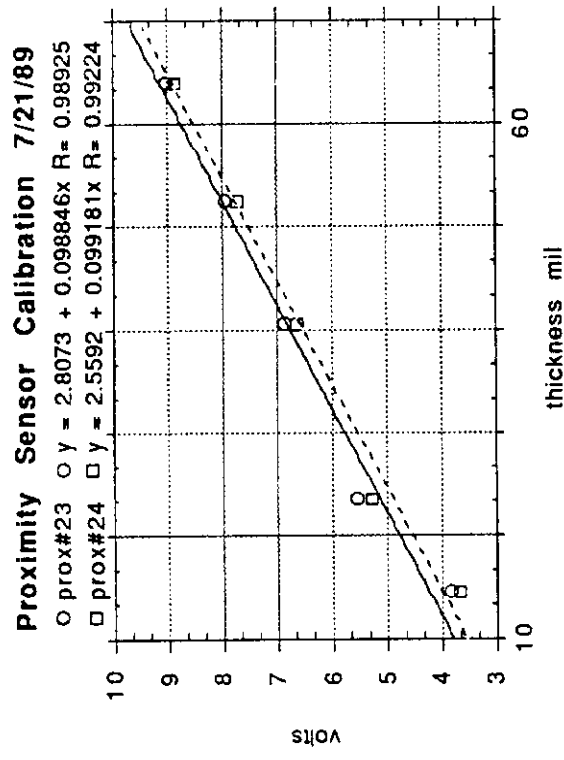
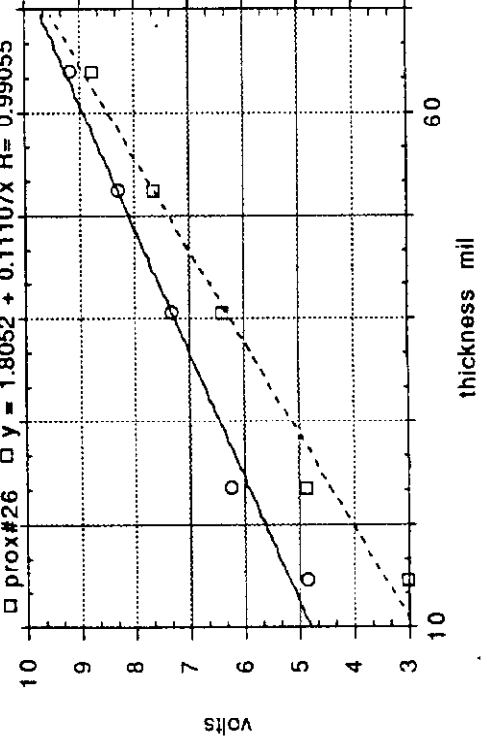
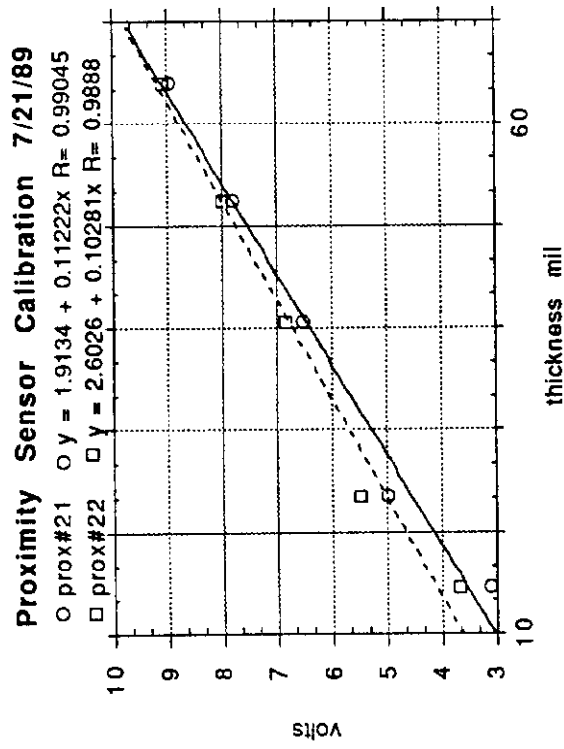


Fig. 13 Proximity Sensor Calibration and Linearity

Once the proximity sensors were calibrated and their ranges set, they were placed in the positions shown in Fig. 11 at distances which yielded an output reading in the middle of their calibrated ranges.

#### 4.2 Temperature IC calibration

The temperature sensor offsets were also calibrated. A fan was used to move air through the chamber with no heat added or water moving through the channels. It was assumed that under these conditions the temperature in the chamber would become uniform. Temperatures were recorded for all of the sensors for 2 hours after the chamber had been allowed to reach thermal equilibrium. Then the average temperature for each sensor was figured. The resulting temperatures were averaged over all sensors to obtain a "best fit" temperature. The offsets necessary for each sensor to read the same under these conditions was then figured and are listed below

SENSOR	OFFSET	SENSOR	OFFSET
1	0.7902	6	0.7172
2	-1.2088	7	0.5692
3	-1.2708	8	0.0052
4	-0.718	9	-0.2058
5	0.4942	10	0.1812

The offsets were programed into the scanning program, which reads each sensor, subtracts the offset and reports the result as the temperature. The same method and calibration was performed for the "water in" and "water out" temperature sensors. The offsets were +.36255, and -.36255 respectively. These offsets were used until 8/10/89. Then we checked the sensors directly for AC voltages. It was observed that all temperature channels were giving readings of approximately 130 mV-AC (thought to have been picked up by the heater strips). We do not think that the AC noise would invalidate any of the conclusions or results formed to this time, but the circuit was modified anyway. A 10k ohm load resistor was added to each circuit to reduce the effect. The resistor in the circuit dropped the ac voltage to almost zero but also affected, by an average of 2.5 F°, the readings of the sensors on the dc scale. This required the recalibration of all the sensors. The process was repeated and new offsets calculated. The following values are reflected in all readings after 8/10/89.

SENSOR	OFFSET	SENSOR	OFFSET
1	0.0285	6	0.3393
2	-0.2915	7	0.3834
3	-0.2963	8	-0.0176
4	-0.2034	9	-0.4509
5	0.2064	10	-0.3441

## 5. Data and Analysis

The measurements and calculations have had two aspects, mechanical and thermal. Although data on both have been taken simultaneously they will not be presented that way. Data related to the stiffness and movement of the chamber will be presented in Chapter 6. Thermal aspects of the experiment will be discussed in Chapter 7.

## 6. Chamber Rigidity Studies

In the initial phase data were taken under a variety of conditions with heat/no heat, with/without water cooling and with three different fans. These data are available in the log books, but are now superseded by the more recent data shown below.

### 6.1 A Six-Day Run with Heat, Air and Water Cooling

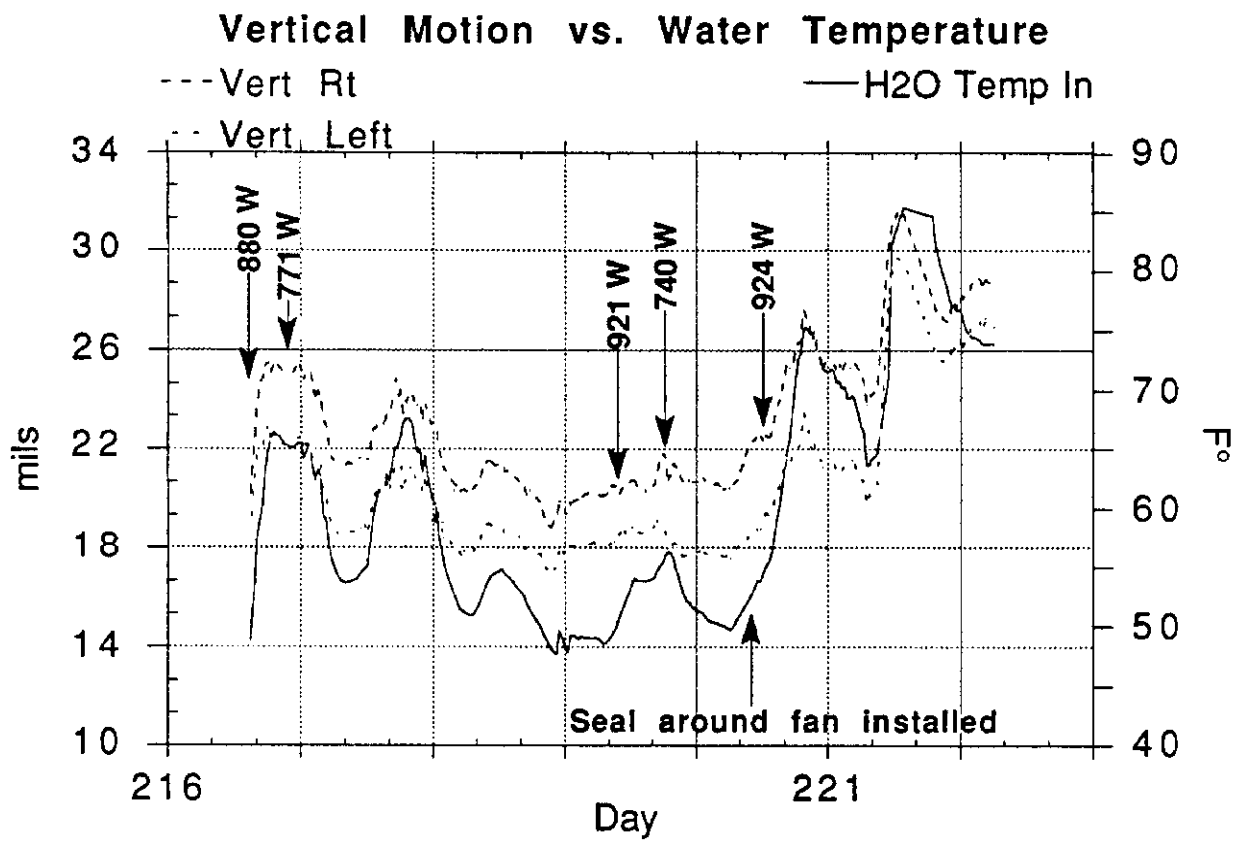
We show data (Scan 8/4 - 8/10/89) recorded over a six day period and a variety of conditions. The brass model was supported by two thick stands for this run.

Fig. 14 shows two vertical sensor traces and a graph of the water temperature for the six days of the run. We note that

1. The vertical movement ranges over 12 mils, which is uncomfortably large.
2. The vertical movement is slow, over a period of hours typically
3. The vertical movement parallels the water temperature.

Fig. 15 shows the horizontal and rotational motion. The horizontal motion stayed mostly within a band of about 2 mils until conditions were changed as to heating power and the effectiveness of the fan. On day 220.5 we stuffed foam rubber around the fan coupling to the chamber to reduce blow-back and to increase the air flow through the chamber. This resulted in a 6 mil horizontal shift. Part of this shift may have come from mechanical pressure of the foam rubber against the chamber. The relaxing right after that time supports that hypothesis. When the water was turned off on day 221.5 there was a 10 mil shift in the opposite direction, again followed by very little motion once the new conditions had been established.

The rotational motion (Fig. 15b) was obtained from a pair of horizontal sensors at the top and bottom of the chamber. The total angular swing is about 200  $\mu$ rad, corresponding to about a 1 mil sideways motion at the sensor locations.



**Fig. 14 Vertical Motion and Water Temperature, 6-Day Run**

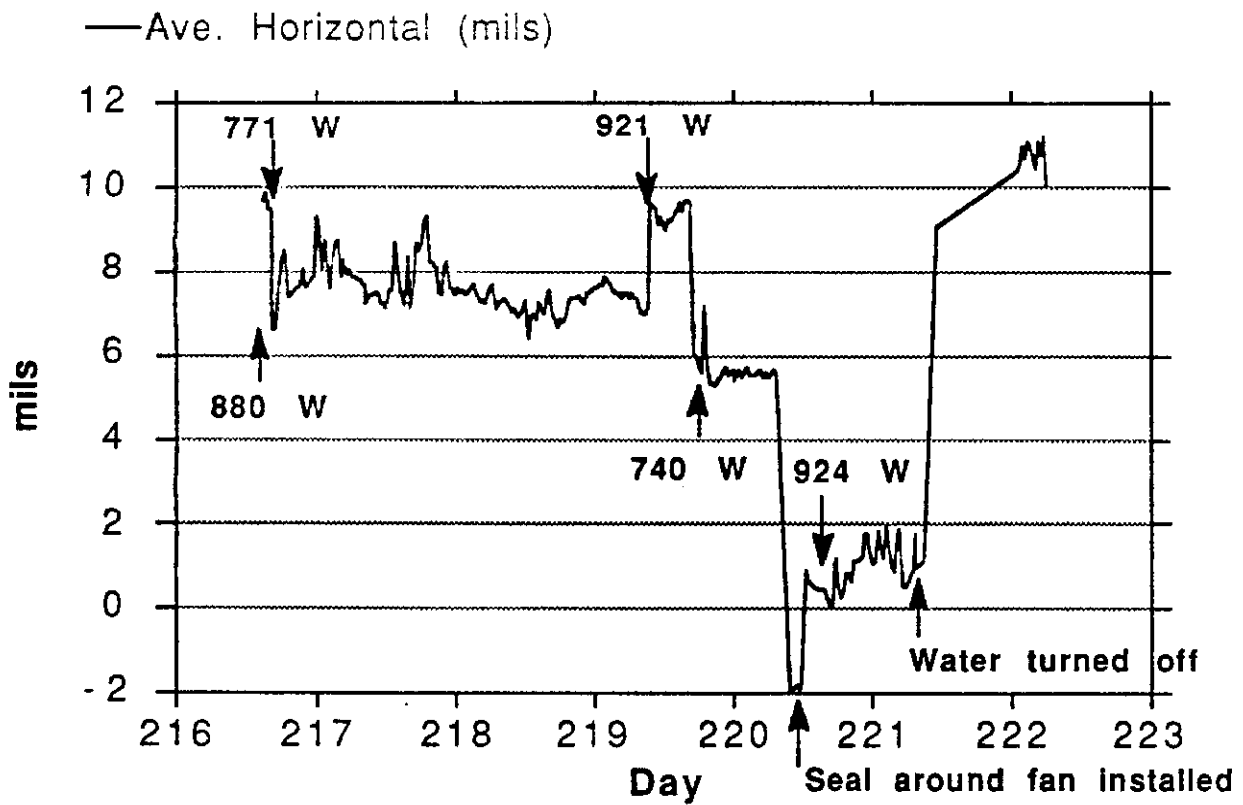


Fig. 15a Horizontal Motion, 6-Day Run

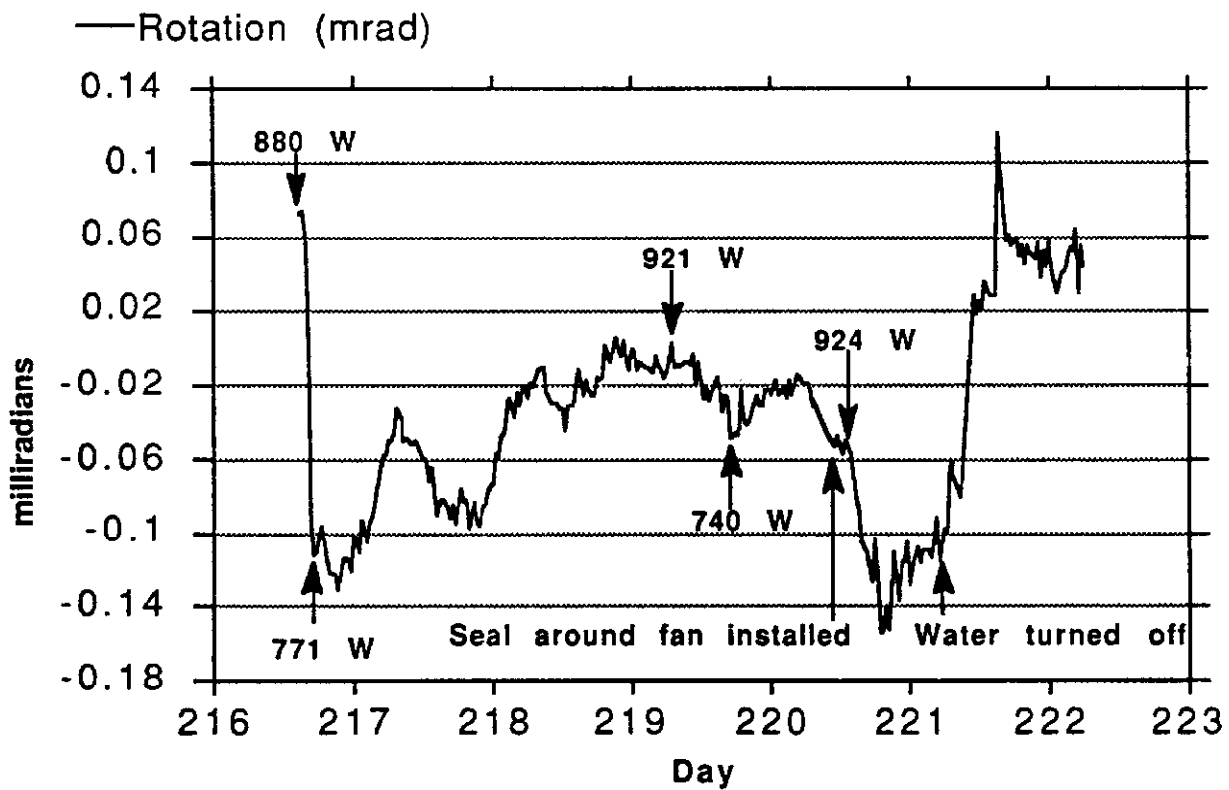


Fig. 15b Rotational Motion, 6-Day Run

## 6.2 Correlation of Vertical Motion with Temperature

Part of the vertical motion may be understood by looking at the differential expansion of the brass structure versus the steel table. The brass expands at a higher rate than the steel table ( see Fig. 6;  $20 \times 10^{-6}$  per C for brass versus  $15 \times 10^{-6}$  per °C for steel). Since the footings of the aluminum end plates were epoxied to the steel table, expansion of the brass will induce a bend moment into the brass structure, leading it to bow upward. Thus at higher temperature the vertical position goes up as seen in the graphs.

Fig. 16 shows the vertical position and the temperature difference between the brass and the steel table as a function of time. Since most of the temperature variation comes from the meanderings of the cooler unit this graph looks much like the one in Fig. 14., although the tracking might be a little closer. Again, there is a clear correlation , with a variation of only 2 to 3 mils (with the exception of a few data points around day 220.5).

## 6.3 The Flexible Stand

Tests are now running with a modified stand. One of the stiff aluminum end plates (the downstream one) has been replaced with one made from 1/16 inch aluminum sheet to avoid bending the brass structure. Results are shown in Figs. 17 and 18.

Fig. 17 shows the motions during this run, which had a heating power of 880 W, water cooling on and air cooling with the large blower. We see now much smaller motions, i.e.

0.8 mils in the vertical plane

about 1 mil maximum in the horizontal plane

The motions were this small in spite of air and water temperature swings of about 8 °F, as seen in Fig. 18. This figure also shows that the remaining vertical motion is still strongly correlated with the steel/brass temperature difference, tracking it at the 0.2 mil level. This gives hope that the motion could be reduced even further in the future.

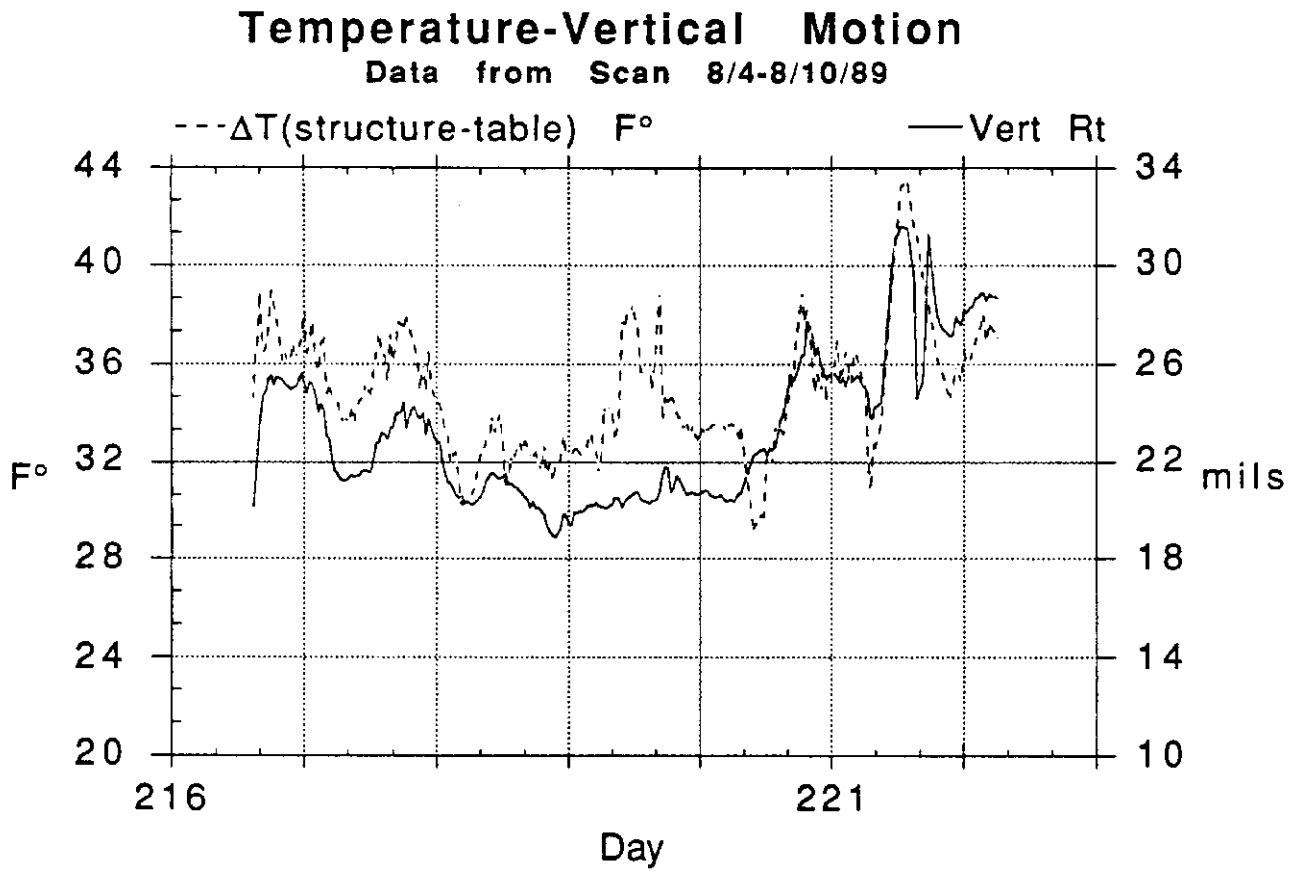


Fig. 16 Vertical Motion and  $\Delta T$  (Brass - Table)

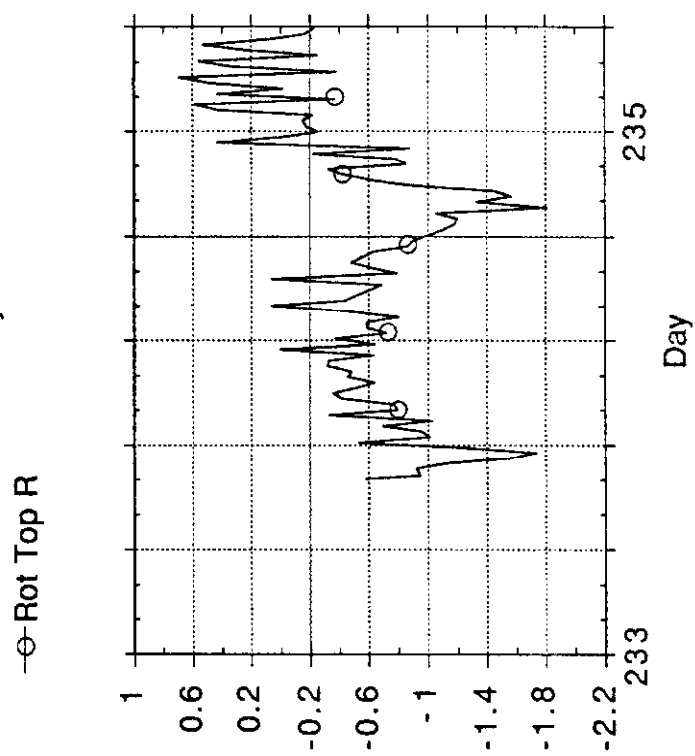
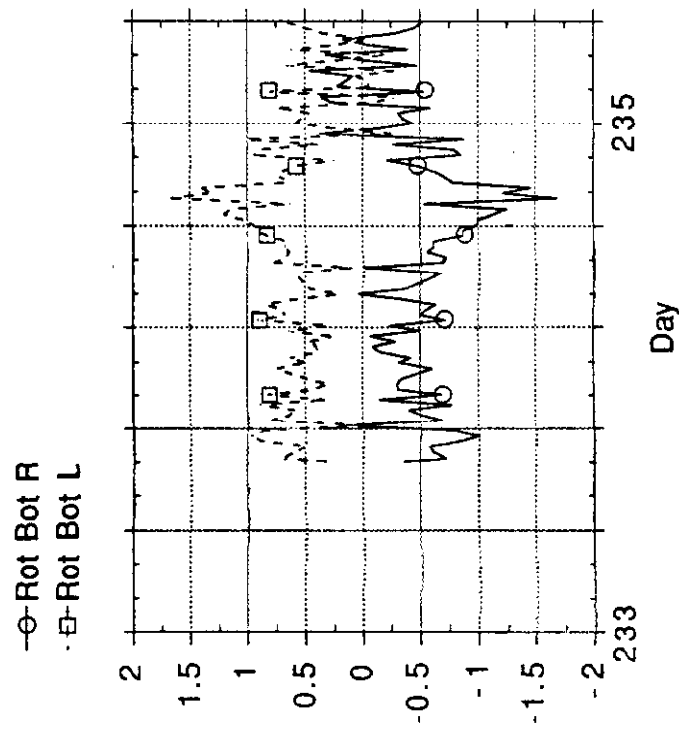
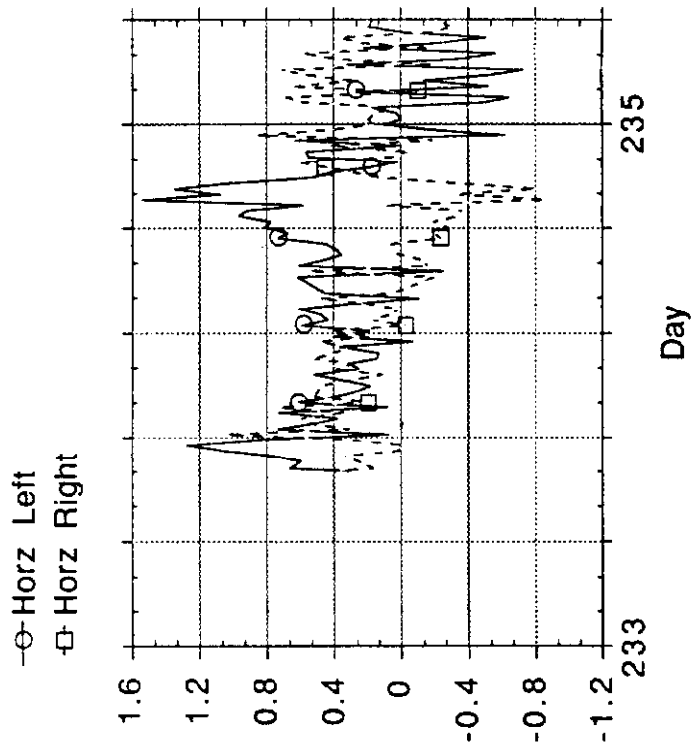
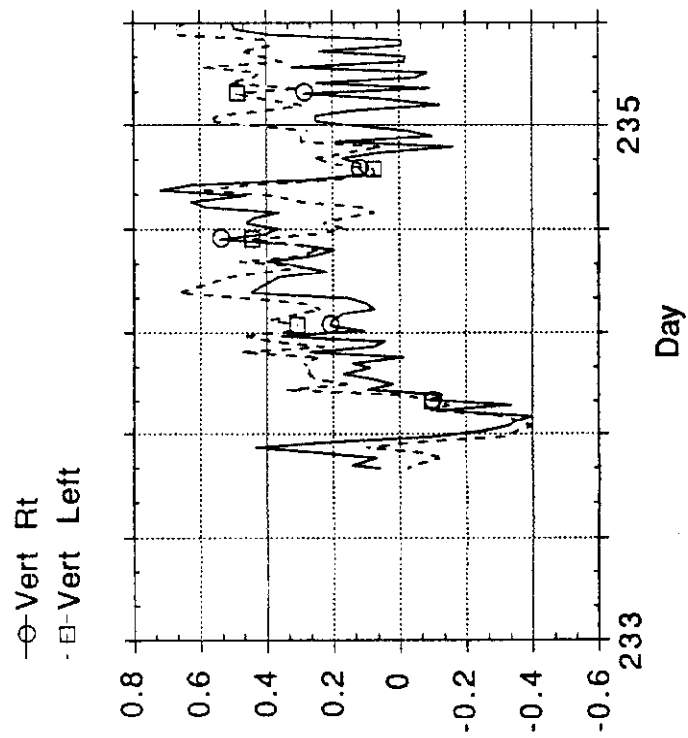
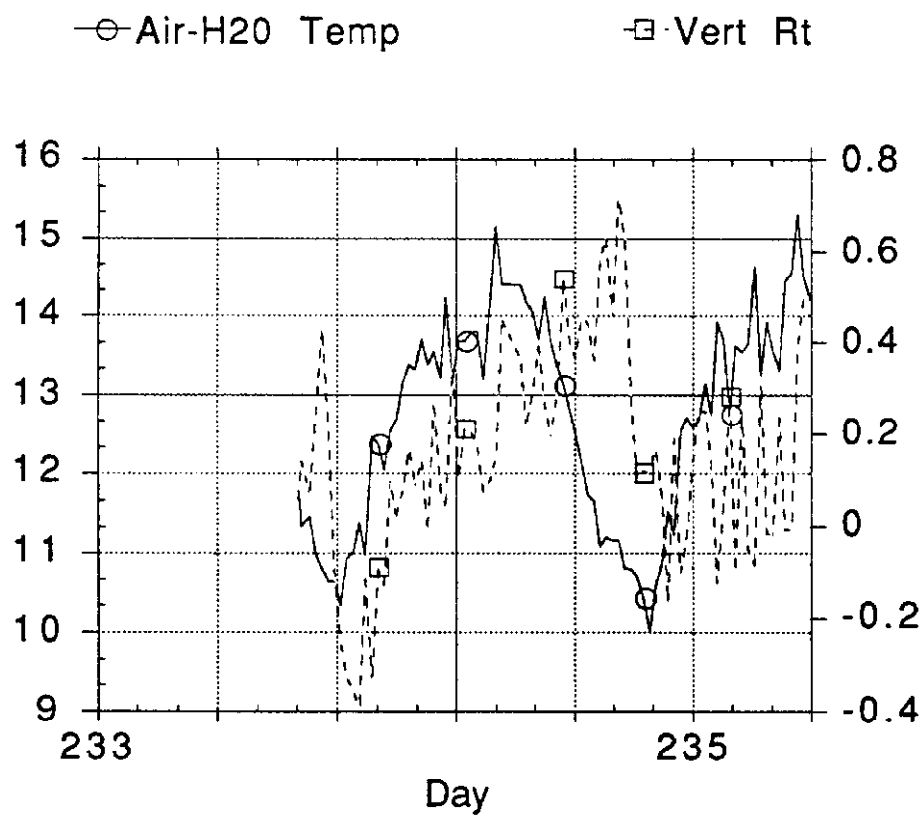
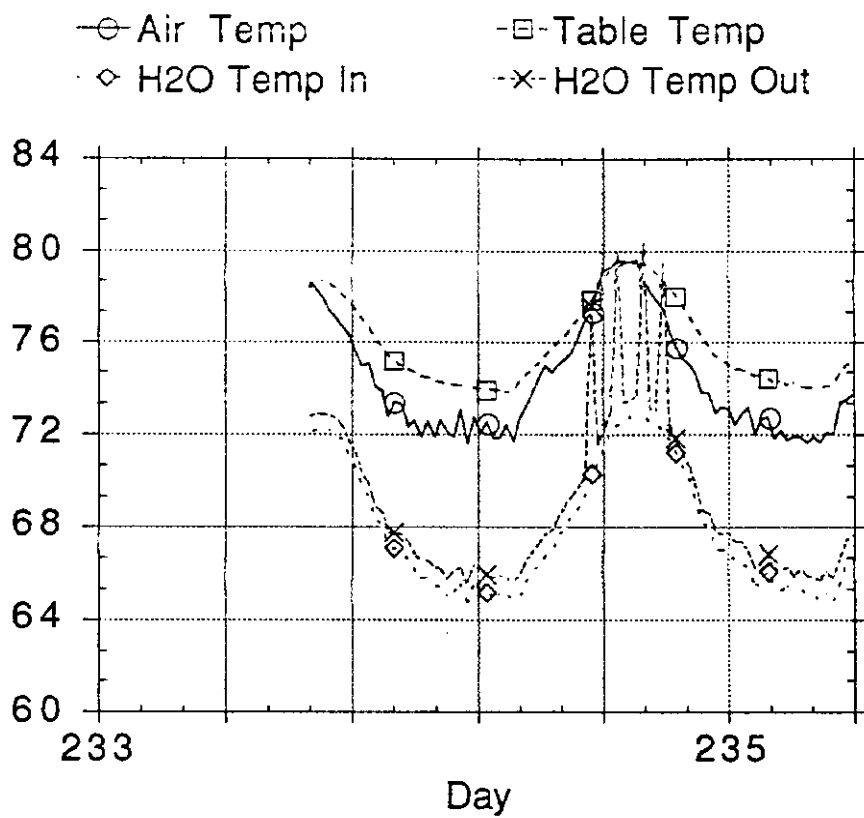


Fig. 17 The Flexible Stand--Motions



**Fig. 18 The Flexible Stand--Temperatures**

## 6.4 Compliance

The last item that will be discussed relative to the stiffness of the chamber is the compliance. We placed known masses on the top of the chamber and read the vertical proximity sensors to determine how much the chamber dropped due to the weight of the mass. The results are shown in Fig. 19 and the numbers are listed below. The left and right sensors gave slightly different results, probably due to nonlinearity and to calibration errors of the two proximity sensors. Taking the reciprocals of the average slope of the two readings for a measure of strength gives

for sensor #21                       $(0.0012171 \text{ mils/g})^{-1}$  or 822 g/mil

for sensor #25                       $(0.0013057 \text{ mils/g})^{-1}$  or 766 g/mil

It should be remembered that the modulus of brass (as used in this model) is only 38% of that of beryllium, to be used in the proposed BCD detector.

## 7. Thermal Studies

The silicon detector support structure must

1. carry away the heat produced by the amplifier chips, while maintaining an acceptable temperature for the silicon chips
2. keep temperature induced motion to acceptable levels.

The first goal, to cool the chips, can be thought of as consisting of several steps:

1. Heat transfer from the chip to the air ("air" is used generically for the gaseous cooling medium), and
2. Maintenance of an acceptable air temperature, either by moving sufficient amounts of air flow or by re-cooling the air along the way.

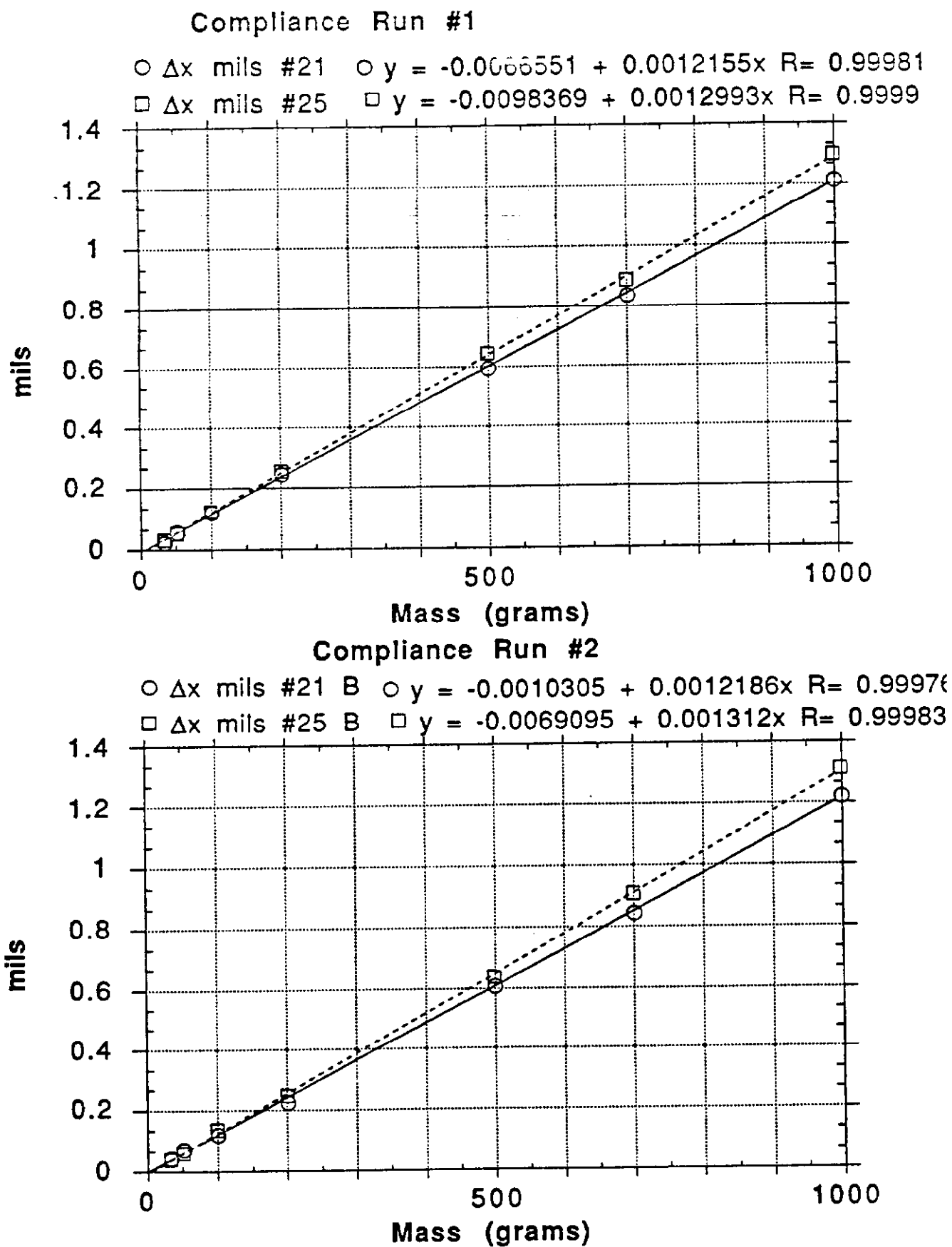


**Fig. 19 Compliance Data and Fits**

To this date we have only studied the overall air temperature rise, with and without water re-cooling, and the temperature induced motions. This is because the interior of the model so far has only webs, not modules. Modules are expected to increase the air flow resistance and affect the heat transfer to the water. We are planning for the next phase to have an instrumented module plus a number of "fake modules" installed to accomplish the missing studies.

### **7.1 The Heat Load**

The electronic amplifier and readout chips, mounted directly on the silicon wafers, will generate a lot of heat. Figure 20 shows statistics prepared by Carl Lindenmeyer on the power that will be dissipated by the channel chips. As can be seen from the figure the heat load is estimated to be between 2121 - 2439 W if one assumes 2.0 mW per channel. It is hoped that when the detector is actually built the state of the art electronics will actually be 1.0 mw per channel. This would then generate a heat load between 1056 - 1220 W. Since the heat strips in the brass chamber will dissipate around 1000 watts at 120 V the experiments here should have direct applicability to the actual detector.

The first concern involving the heat that was addressed through experimentation was the temperature difference throughout the chamber. While there are no established specifications, we think that a temperature rise of the air of around 5 °F would be desirable with a range of up to 10 °F being perhaps acceptable. A fan moves the air along the axis of the support structure. The chamber air can be re-cooled by thermal contact with cool water(a generic term for any cooling fluid) flowing through channels along the structure. This is in Fig. 21:

3-5-89

# BCD SILICON VERTEX DETECTOR

	CENTRAL STATIONS	FRWD. STATIONS (BOTH ENDS)	TOTAL
Nº OF MODULES	10	18	28
Nº OF DISCS PER MODULE	2	2	
DISC SPACING	24 MM	15 MM	
Nº OF DIFFERENT SILICON PIECES	5	1	6
Nº OF 100MM SILICON WAFERS	380	216	596
Nº OF 128 CHANNEL CHIPS/MODULE	456	276 (207)	
Nº OF 128 CHANNEL CHIPS	4560	4968 (3726)	9528 (8286)
Nº OF CHANNELS	583,680	635,904 (475,928)	1,219,584 (1,060,608)
Nº OF CABLES PER MODULE	84	24 (18)	
Nº OF CABLES	840	432 (324)	1272 (1164)
HEAT LOAD @ 2MW PER CHANNEL	1167 WATTS	1272 (954) WATTS	2439 (2121) WATTS
	3990 BTU/HR	4349 (3262) BTU/HR.	8339 (7252) BTU/HR.

NUMBERS IN PARENTHESIS INDICATE UN-INSTRUMENTED REDUNDANT STRIPES IN FORWARD STATIONS

Fig. 20 Heat Loads for the BCD Silicon Vertex Detector

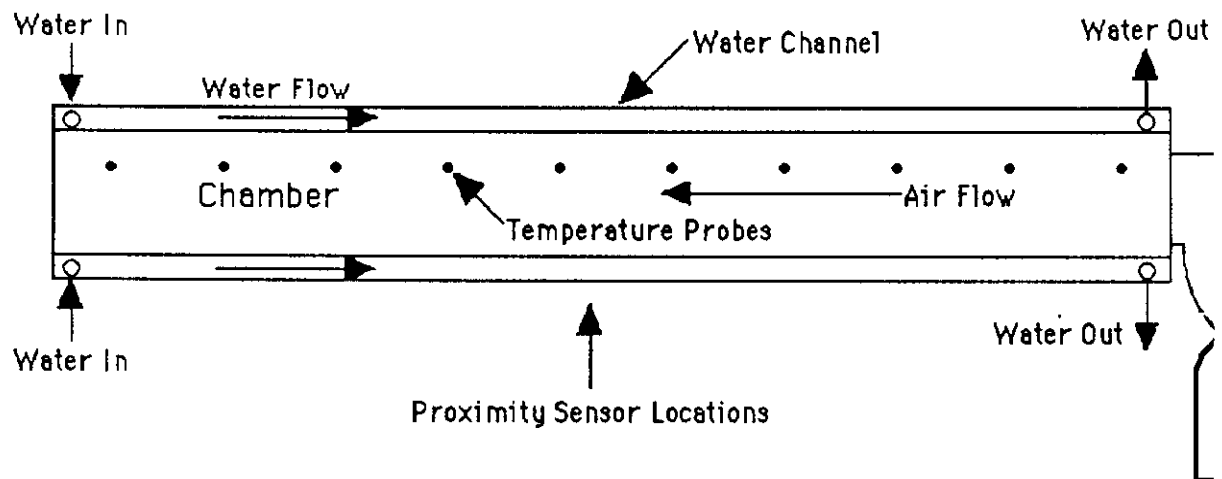


**Fig. 21 Air and Water Flow through the Model**

Some of the heat will be conducted through the brass walls to the cooler water moving through the water channels . In comparing the heat conductivities

Heat Conductivity of Beryllium = 87 Btu-ft/hr-ft<sup>2</sup>-°F

Heat Conductivity of Brass = 70 Btu-ft/hr-ft<sup>2</sup>-°F

one can see that the conductivity of the brass is 79% of the beryllium that will be used. While brass will not have quite the same ability to cool the chamber air as beryllium, the two materials are sufficiently close for the present studies.

## 7.2 Water Flow Rate Measurements

The flow rate of water determines its temperature gain for a given heat input. We used a bucket and a stop watch to record the time it took the pump to put varying amounts of water. The weights shown were determined on a Toledo scale with 0.5 lb. graduations.

<b>Trial</b>	<b>Weight of Water</b> (pounds)	<b>Time</b> (sec)	<b>Flow Rate</b> lb/s
1	18.1	145.18	0.125
2	21.6	206.18	0.105
3	23.0	215.53	0.107
4	22.5	211.72	0.106
5	21.1	204.28	0.103

The flow rate in lbs/s was calculated by dividing the weight of the water by the time. The last four values were averaged to 0.105 lbs/s then converted to 48 g/s using 454 g to a pound.

To get an idea of the cooling 'power' of the water multiply the flow rate of the water times the specific heat of water times the temperature difference of the water between entering and leaving the channels. For example:

$$\begin{aligned}
 P &= c \text{ (m/t)} \Delta T \\
 &= (1 \text{ cal/g-}^\circ\text{C}) (47.67\text{g/s}) (1 \text{ }^\circ\text{C}) (4.19 \text{ J/cal}) \\
 &= 200 \text{ J/s} = 200 \text{ W}
 \end{aligned}$$

As can be seen for each 1.0 °C, or 1.8 °F, the water temperature drops in the channel, one can expect 200 watts of cooling power.

### 7.3 Air Flow Rate for Three Different Fans

The air flow rate of the fans used is difficult to measure directly because of the low pressure drops and the uneven flow profile across the apertures. We used a thermal method to estimate the air flow rates.

When running without any water flow, we assume that most of the heat is carried by the air stream, not through the sides of the brass model. Knowing the electric heat input we can find the air mass flow from the measured temperature rise of the air stream:

$$\begin{aligned} \text{Power } P &= c (m/t) \Delta T & c &= \text{specific heat of air (0.2214 cal/g } ^\circ\text{C)} \\ m/t &= P / (c \Delta T) & m/t &= \text{mass flow rate of air} \\ & & \Delta T &= \text{temp. rise of the air} \\ & & \text{Conversion factor} &= 4.185 \text{ J/cal} \end{aligned}$$

<u>Fan</u>	<u>Power</u>	<u><math>\Delta T</math></u>	<u>m / t</u>
Boxer	402W	32 $^\circ\text{F}$	24 g/s
Centrifugal	938 W	16.1 $^\circ\text{F}$	58 g/s *
Turbine	970 W	8.78 $^\circ\text{C}$	120 g/s

\* It should be noted that at the time these measurements were made the fan was sealed to the chamber.

### 7.4 Heat Transfer into the Water

The heat transfer into the water (K in Watts/ $^\circ\text{C}$ ) depends on the flow rate of the fans and the temperature difference between the air and the water.

This can be clearly seen in Fig. 22, where the air and water temperature gains are plotted (with two different scales) against time for the 6-day run. Whenever the water temperature dropped, more heat was accepted by the water stream, and hence less  $\Delta T$  was created for the air stream, hence the mirror-image quality of the traces.

The heat transfer should be proportional to the air/water temperature difference since the flow pattern is forced by the fans, not by heat driven convective currents. We derive a heat transfer coefficient  $K$  (in watts /Celsius) from the temperature rise measured with each of the three fans that have been used in this investigation:

$$(C_{H_2O}) (\text{flow rate of } H_2O) (\Delta T_{H_2O}) = K (T_{\text{ave. air}} - T_{\text{ave. } H_2O})$$

$$(1 \text{ cal/g}^\circ\text{C})(47.67 \text{ g/s})(4.19 \text{ J/cal})(\Delta T_{H_2O}) = K (T_{\text{ave. air}} - T_{\text{ave. } H_2O})$$

$$K = (199.74 \text{ W/}^\circ\text{C})(\Delta T_{H_2O}) / (T_{\text{ave. air}} - T_{\text{ave. } H_2O})$$

The  $(\Delta T_{H_2O})$  and  $(T_{\text{ave. air}} - T_{\text{ave. } H_2O})$  temperatures (in  $^\circ\text{C}$ ) were determined from the measurements taken over a period of days for each type of fan.  $K$  was determined by plotting  $(\Delta T_{H_2O})$  vs.  $(T_{\text{ave. air}} - T_{\text{ave. } H_2O})$  and fitting the best straight line using KaleidaGraph. The results are shown in Figs. 23 and are tabulated below:

<u>Fan</u>	<u>m / t</u>	<u>K</u>
Boxer	24 g/s	4.6 W/ $^\circ\text{C}$
Centrifugal	58 g/s	17 W/ $^\circ\text{C}$
Turbine	120 g/s	16.2 W/ $^\circ\text{C}$

While there is a large increase in the heat transfer coefficient in going from the weak Boxer fan to the Centrifugal Blower, presumably due to increased turbulence, there is no further increase for the Turbine. The measurements of  $K$  are a useful guide for now, but they will have to be repeated when modules are installed in the support structure.

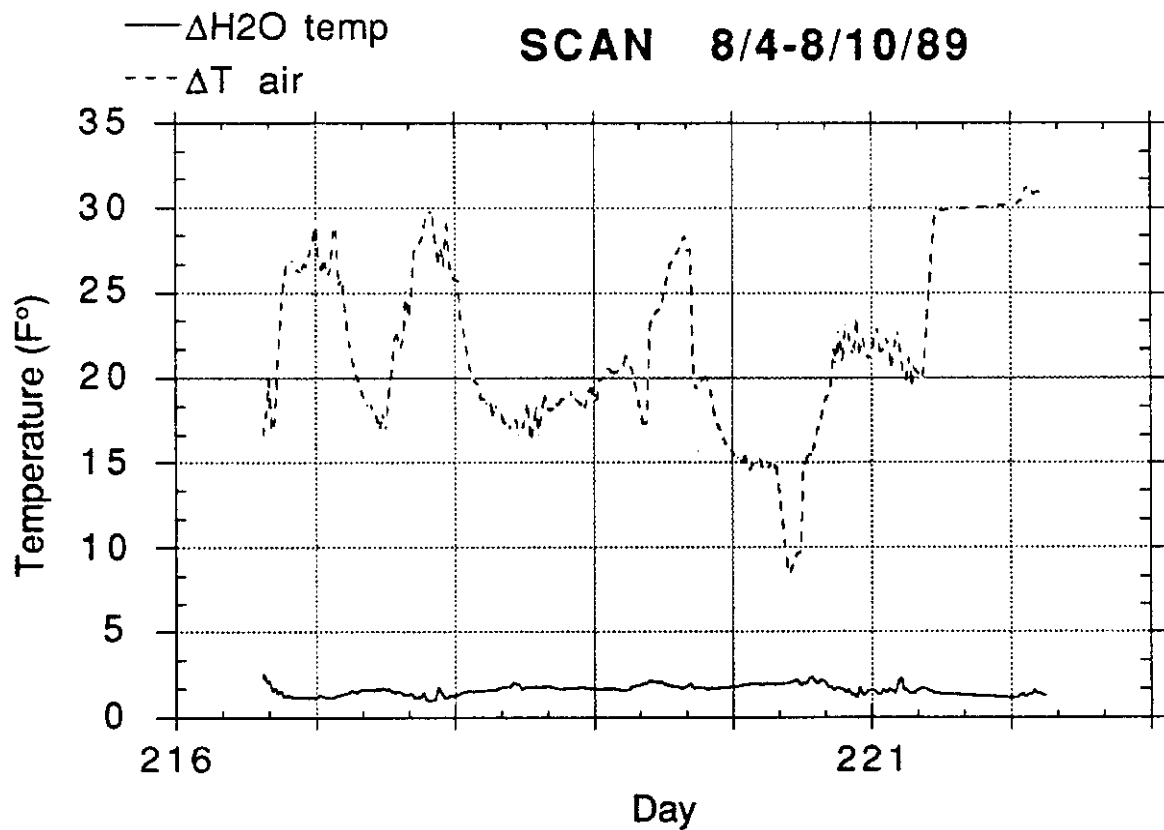
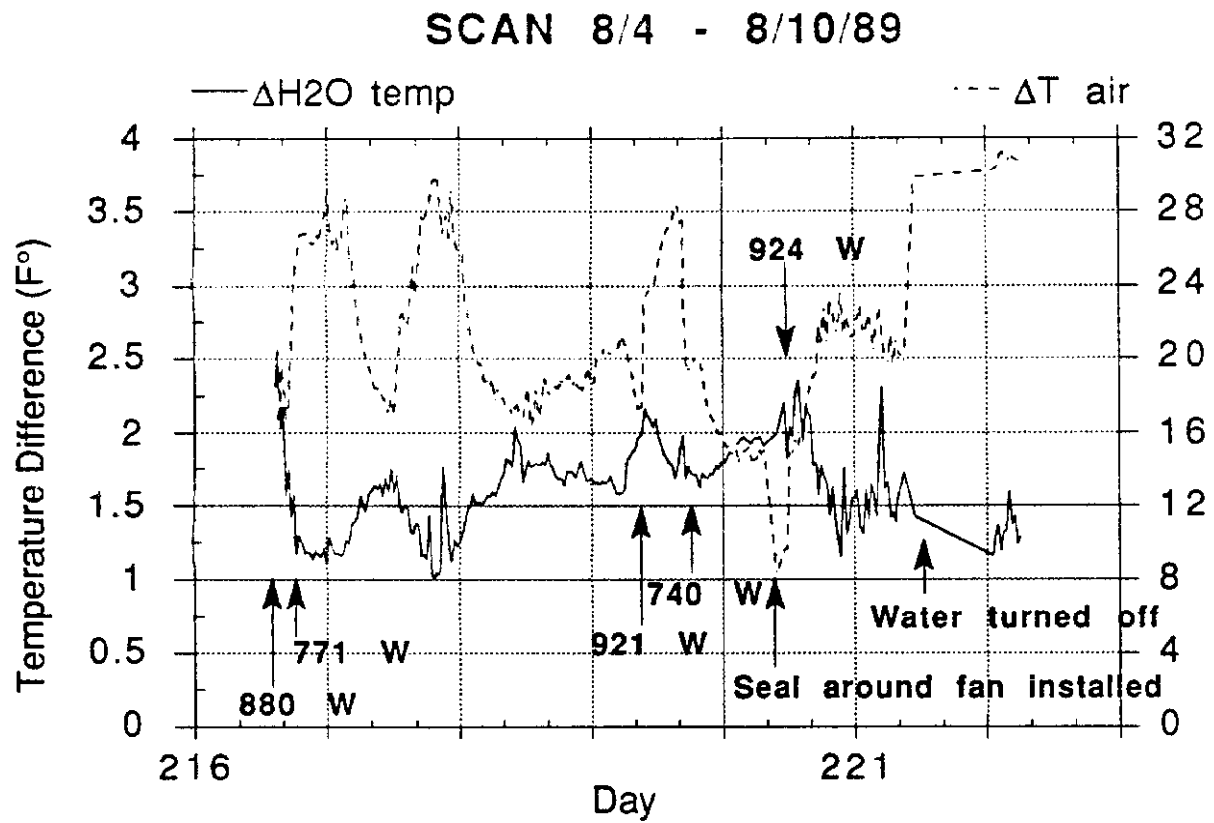


**Fig. 22     $\Delta T$  for Air and Water Streams during 6-Day Run**

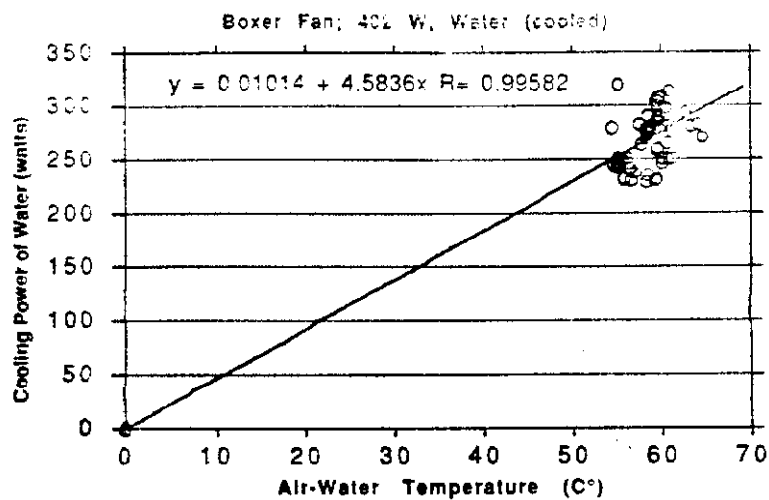


Fig. 23a Heat Transfer into Water for the Boxer Fan

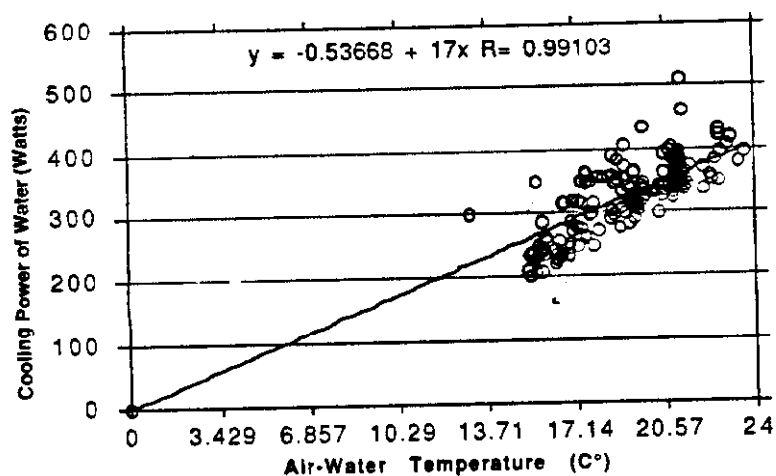


Fig. 23b Heat Transfer into Water for the Centrifugal Blower

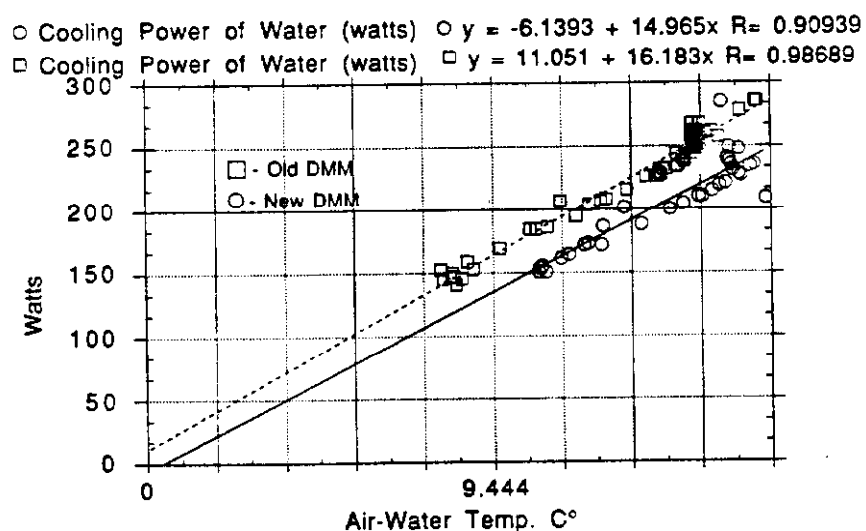


Fig. 23c Heat Transfer into Water for the Turbine

## 7.5 Temperature Profiles

Figs. 24a and 24b show the ten temperatures measured in 12" intervals along the brass structure axis. While the temperatures increase as more heat gets carried away by the moving air, each curve tracks the room air temperature quite closely, as expected. The bottom panel of Fig. 24b shows the air and water temperatures for the same 6-day run. The water temperatures were governed by the vagaries of the poorly regulated cooler.

Fig. 25 shows temperature profiles with the boxer fan blowing from end A or end B, respectively. While the general shape of the profiles is as one might expect, the steep rise due to the concentration of heat tapes in the middle is delayed by about 2.5 feet from the center. We believe that this delay means that it will be difficult to cool the concentrated amplifiers in the middle effectively into the water channel. It may be that air cooling will have to be emphasized.

In this regard it is interesting to compare the profiles in Fig. 26, which represent air cooling only (top panel) versus combined air/water cooling (bottom panel). Significant differences occur only toward the exhaust end (right side of graph), where the profile with the added water cooling flattens out as expected.

All statements about the effectiveness of water cooling must be tempered, however, with the caveat that the water cooling must be improved by either lowering the water temperature or by increasing the heat transfer coefficient before one can make a final assessment.

## 7.6 Examples of Temperature Rises for Three Fans

The following examples have been calculated based on the measured properties of the model. The purpose is to give an idea of typical operating conditions.

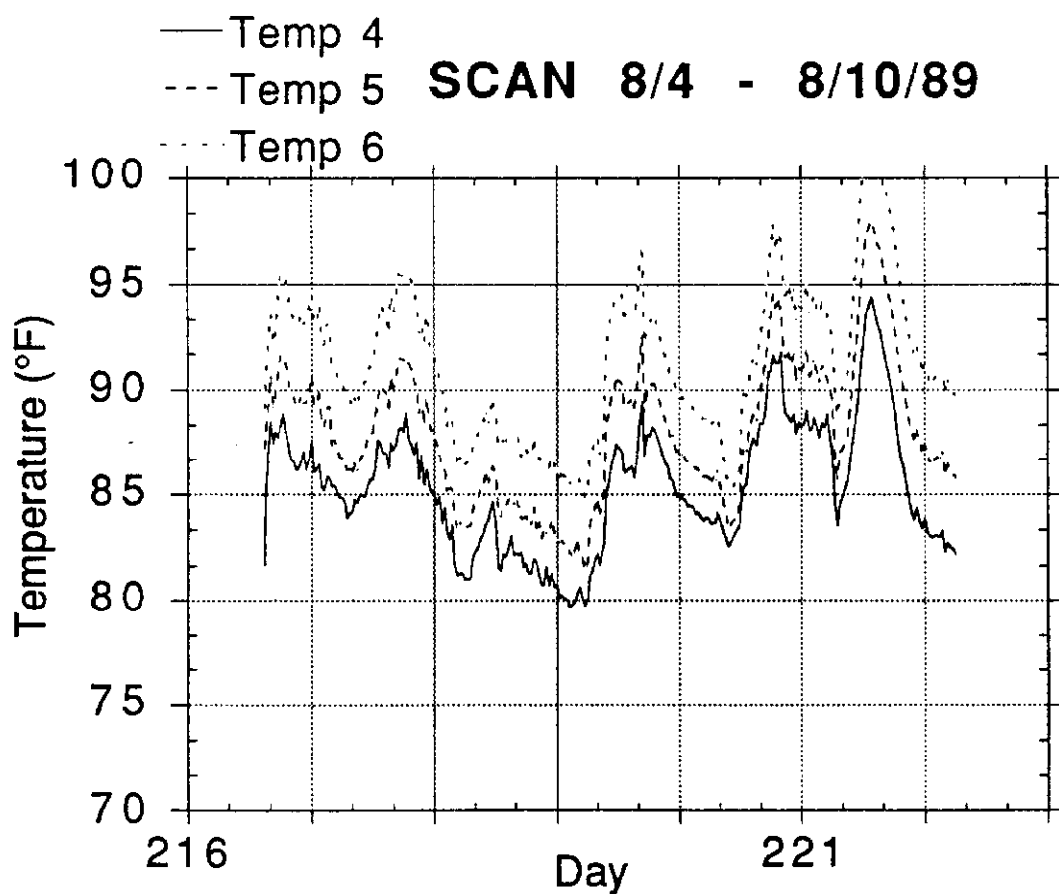
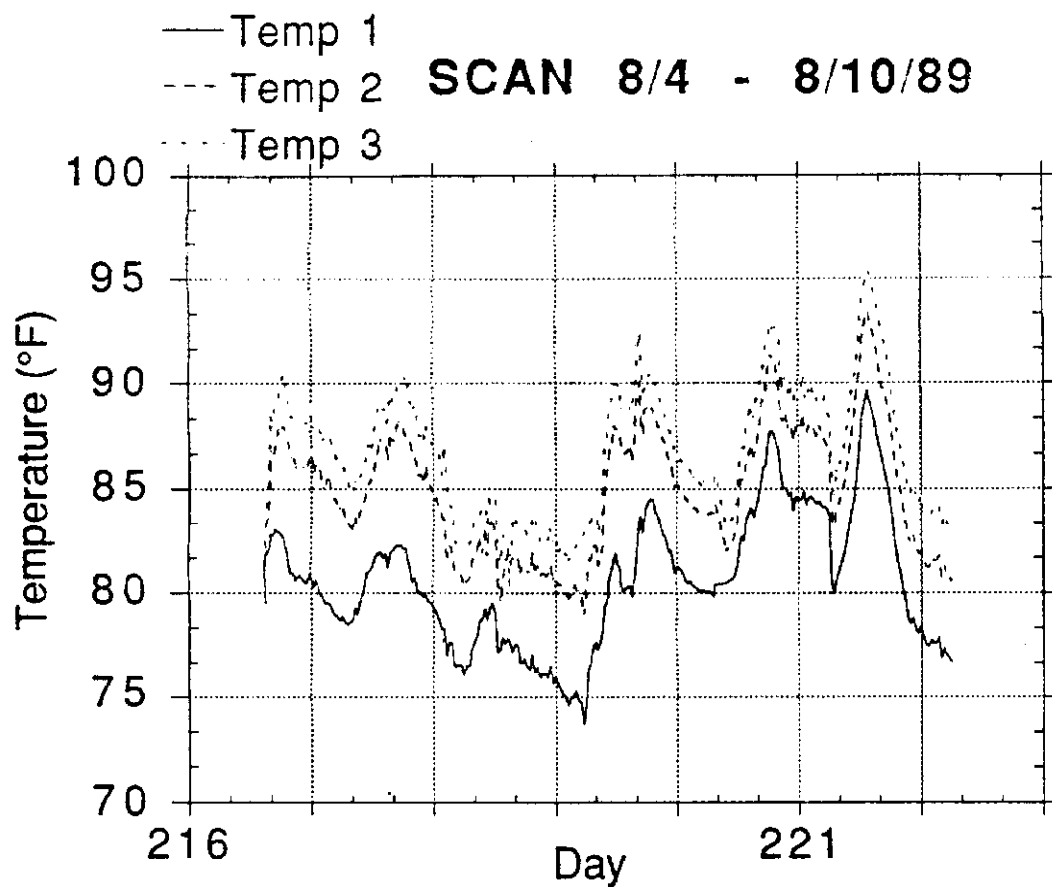


Fig. 24a Temperatures inside the Model versus Time

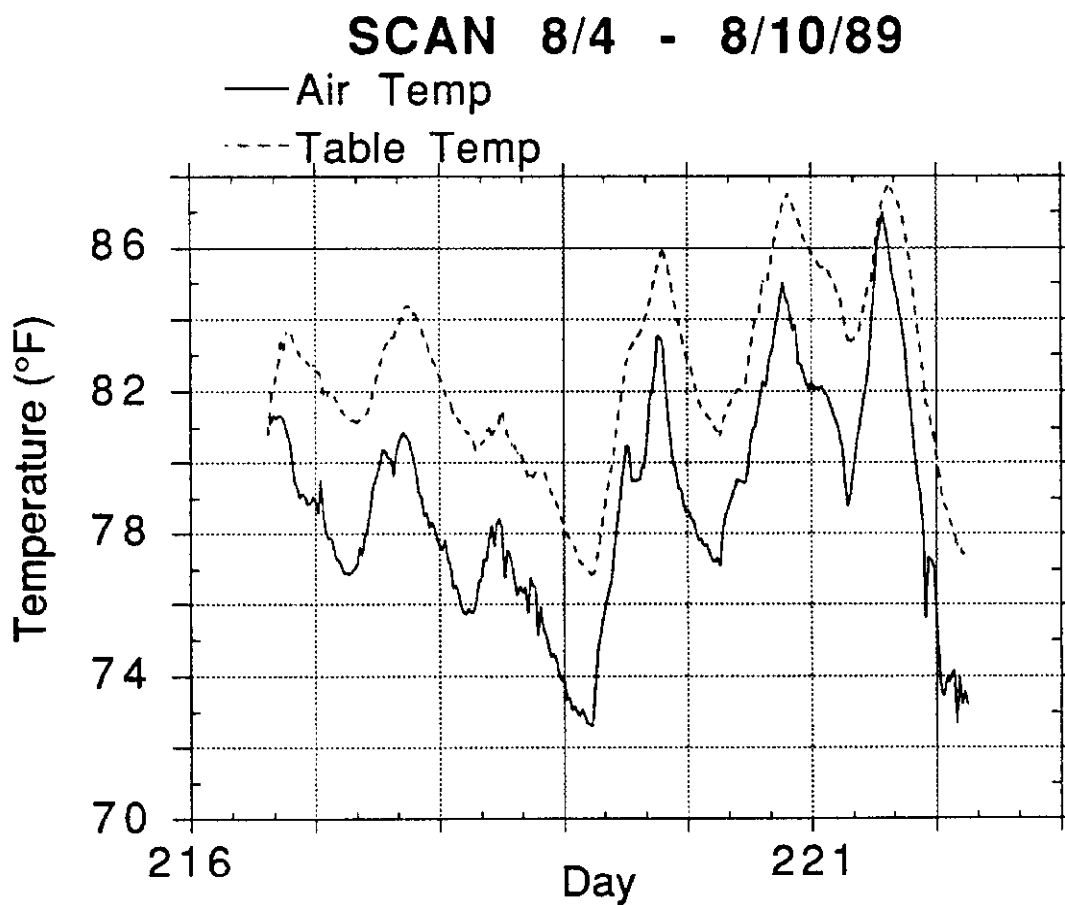
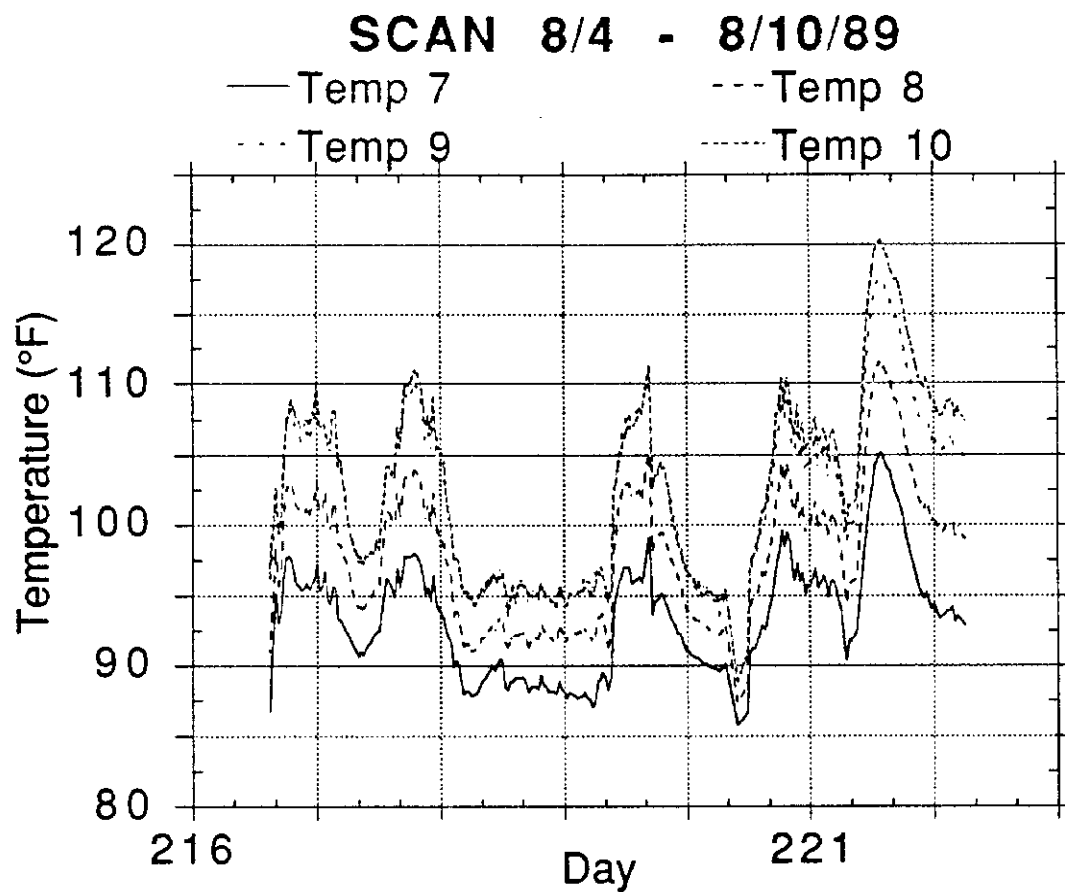
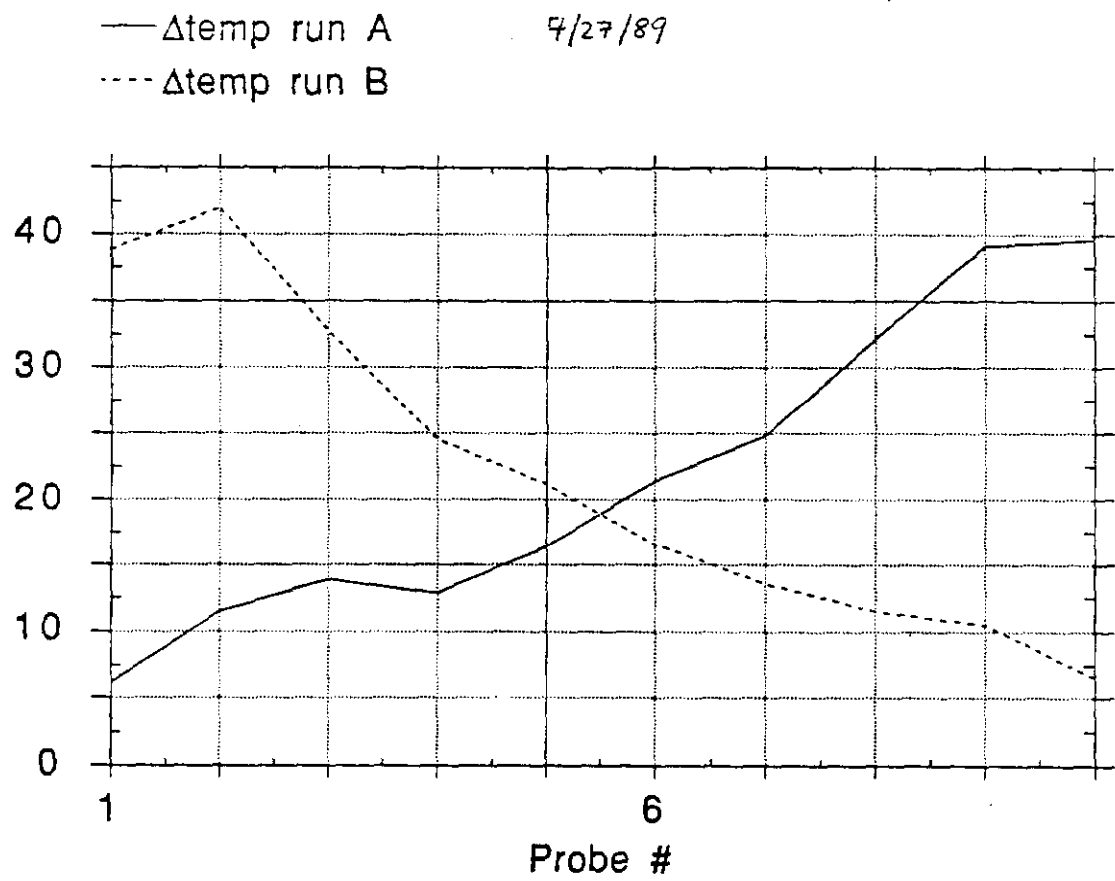
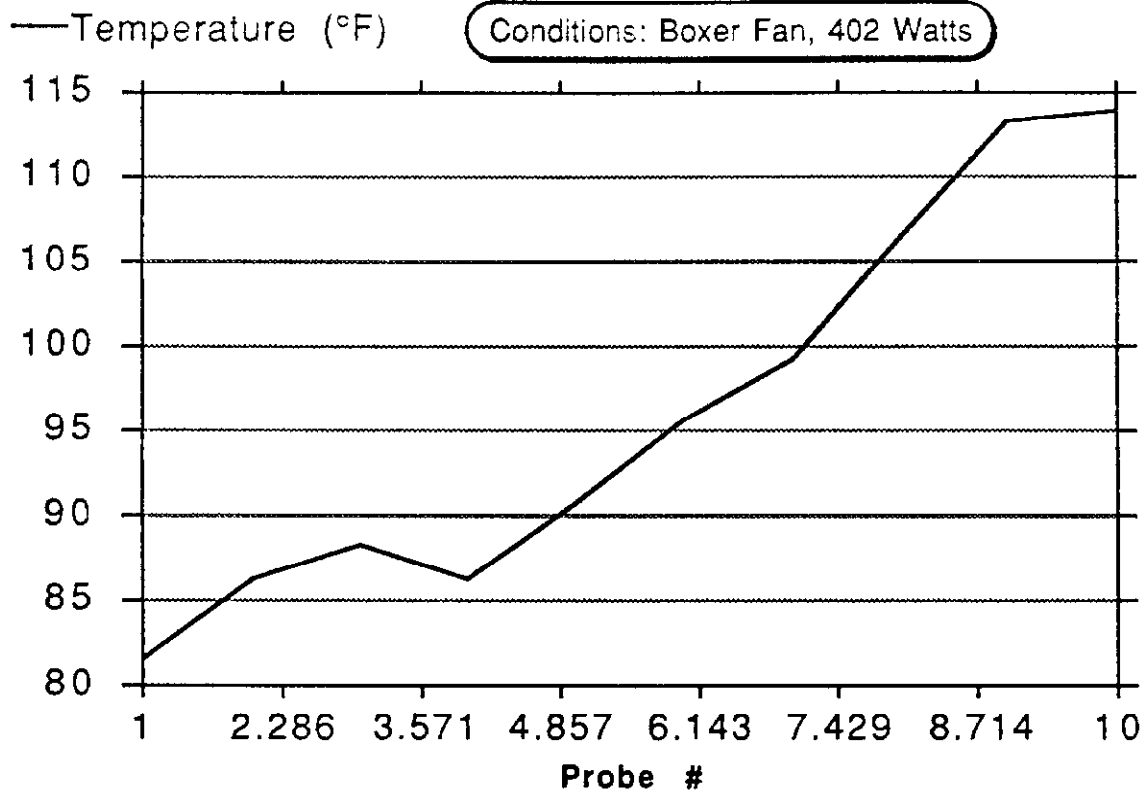


Fig. 24b Temperatures inside the Model versus Time



**Fig. 25    Temperature Profiles for two Air Flow Direction**

### Temperature Profile 7/30/89



### Temperature Profile 8/1/89

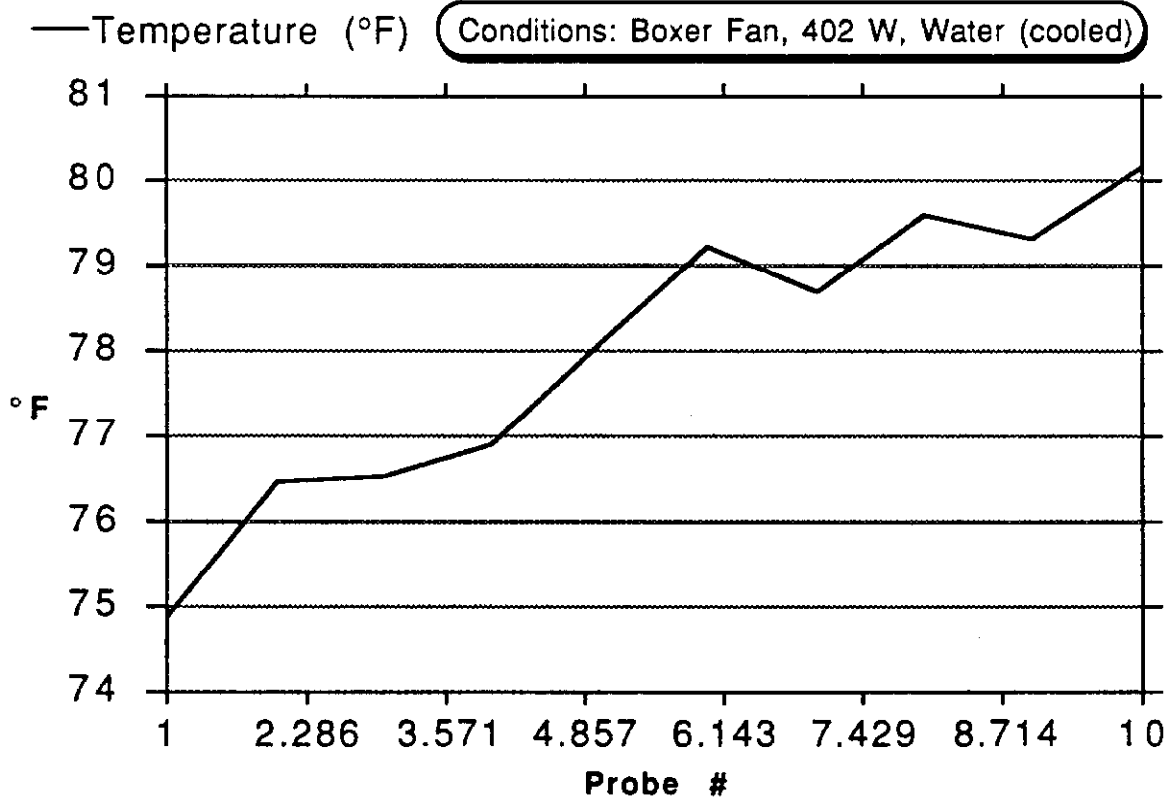


Fig. 26 Temperature Profiles with and without Water Cooling

**A. Air Cooling Only**

<u>Fan</u>	<u>Boxer</u>	<u>Centrif.</u>	<u>Turbine</u>
Mass Flow Rate	24 g/s	58 g/s	120 g/s
Heater Power	1200 W	1200 W	1200 W
$\Delta T$ Air	17.7 °C	7.4 °C	3.6 °C

**B. Air and Water Cooling**

<u>Fan</u>	<u>Boxer</u>	<u>Centrif.</u>	<u>Turbine</u>
Mass Flow Rate	24 g/s	58 g/s	120 g/s
Heat Transfer Coeff.	4.6 W/°C	17 W/°C	16.2 W/°C
Heater Power	1200 W	1200 W	1200 W
Air Cooling Power	600 W	600 W	600 W
$\Delta T$ Air	9 °C	4 °C	2 °C
Water Cooling Power	600 W	600 W	600 W
$\Delta T$ Air/Water	131 °C	35 °C	37 °C

We note that:

1. The air temperature rise with the largest fan, the turbine, is acceptable (3.6 °C with air only and 1.8 °C with air and water cooling).
2. The heat transfer to the water is inadequate at present. It takes a 37 °C differential to drive half the power into the water. Heat transfer can be improved by using additional cooling channels and other design improvements.

## **8. Conclusions**

A brass model of the proposed support structure for the BCD silicon vertex detector has been constructed and tested.

Mechanically, the structure proved to be stable in position at the level of 1 or 2 mils, even in the presence of 1000 W heat input, 120 g/s air flow and 50 g/s water flow.

Thermally, the air temperature rises only 3.6 °C for 1200 W heat input without water cooling, and 1.8 °C with 50% water cooling.

The heat transfer to water cooling must be improved if it is to be used.

The heat transfer to modules and chips on modules has not been studied yet.

Air flow resistance will increase once modules are installed. The measurements reported here will have to be repeated at that time.

## **Acknowledgements**

Hal Mulderink and Neil Michels have worked at Fermilab this summer under the auspices of a program that brings high school science teachers into Fermilab's research environment. This program has been implemented for several years by Dr. Arlene Lennox, to whom I am grateful for spending all that time and energy to make the program such a success and for finding the two outstanding teachers.

The progress detailed in this report would not have come about without the teacher's contribution. Both showed unflagging enthusiasm and considerable knowledge, skill and determination in constructing the apparatus, configuring the measurement system, programming the computer, analyzing the data, drawing meaningful conclusions and writing this report. They have proven to be every bit as skilful in their research work as the old hands here at Fermilab. Either of them is welcome to come back to continue the present work.

We also wish to acknowledge the substantial, continuous competent and very willing support of Jerry Sasek of Lab 6. Jerry has helped us every step along the way in building the model, providing a steel table and working space for these studies and finding blowers for the air cooling studies. This work would not have gotten this far this quickly without Jerry's support.

## **List of Figures**

- Fig. 1      Overview of the BCD Detector**
- Fig. 2      BCD Silicon Vertex Detector, Central Stations**
- Fig. 3      BCD Silicon Vertex Detector, Forward Stations**
- Fig. 4      BCD Silicon Vertex Detector, Forward Stations**
- Fig. 5      BCD Silicon Vertex Detector, Module Mounting Scheme**
- Fig. 6      Coefficient of Thermal Expansion for Various Materials**
- Fig. 7      Arrangement of Reinforcing Webs in the Gutters**
- Fig. 8      Mounting Stand Design**
- Fig. 9      Heating Strip Placement**
- Fig. 10     Air and Water Cooling Configuration**
- Fig. 11     Placement of the Proximity Position Sensors**
- Fig. 12     Schematic of the Data Acquisition System**
- Fig. 13     Proximity Sensor Calibration and Linearity**
- Fig. 14     Vertical Motion and Water Temperature, 6-Day Run**
- Fig. 15a    Horizontal Motion, 6-Day Run**

- Fig. 15b Rotational Motion, 6-Day Run**
- Fig. 16 Vertical Motion and  $\Delta T$  (Brass - Table)**
- Fig. 17 The Flexible Stand--Motions**
- Fig. 18 The Flexible Stand--Temperatures**
- Fig. 19 Compliance Data and Fits**
- Fig. 20 Heat Loads for the BCD Silicon Vertex Detector**
- Fig. 21 Air and Water Flow through the Model**
- Fig. 22  $\Delta T$  for Air and Water Streams during 6-Day Run**
- Fig. 23a Heat Transfer into Water for the Boxer Fan**
- Fig. 23b Heat Transfer into Water for the Centrifugal Blower**
- Fig. 23c Heat Transfer into Water for the Turbine**
- Fig. 24a Temperatures inside the Model versus Time**
- Fig. 24b Temperatures inside the Model versus Time**
- Fig. 25 Temperature Profiles for two Air Flow Direction**
- Fig. 26 Temperature Profiles with and without Water Cooling**